

Spatial second-order positive and asymptotic preserving filtered P_N schemes for nonlinear radiative transfer equations

Xiaojing Xu^{a,b}, Song Jiang^c, and Wenjun Sun^{c,d}

^aSchool of Mathematics and Information Science, Guangxi University, Nanning 530004, Guangxi, China

^bSchool of Mathematics and Physics, Southwest University of Science and Technology, Mianyang 621010, Sichuan, China

^cInstitute of Applied Physics and Computational Mathematics, Fenghao East Road 2, Beijing 100094, China

^dCenter for Applied Physics and Technology, College of Engineering, Peking University, Beijing 100871, China

E-mail : xuxiaojing0603@126.com jiang@iapcm.ac.cn sun_wenjun@iapcm.ac.cn

Abstract

A spatial second-order scheme for the nonlinear radiative transfer equations is introduced in this paper. The discretization scheme is based on the filtered spherical harmonics (FP_N) method for the angular variable and the unified gas kinetic scheme (UGKS) framework for the spatial and temporal variables respectively. In order to keep the scheme positive and second-order accuracy, firstly, we use the implicit Monte Carlo (IMC) linearization method [6] in the construction of the UGKS numerical boundary fluxes. This is an essential point in the construction. Then, by carefully analyzing the constructed second-order fluxes involved in the macro-micro decomposition, which is induced by the FP_N angular discretization, we establish the sufficient conditions that guarantee the positivity of the radiative energy density and material temperature. Finally, we employ linear scaling limiters for the angular variable in the P_N reconstruction and for the spatial variable in the piecewise linear slopes reconstruction respectively, which are shown to be realizable and reasonable to enforce the sufficient conditions holding. Thus, the desired scheme, called the $PPFP_N$ -based UGKS, is obtained. Furthermore, we can show that in the regime $\epsilon \ll 1$ and the regime $\epsilon = O(1)$, the second-order fluxes can be simplified. And, a simplified spatial second-order scheme, called the $PPFP_N$ -based SUGKS, is thus presented, which possesses all the properties of the non-simplified one. Inheriting the merit of UGKS, the proposed schemes are asymptotic preserving. By employing the FP_N method for the angular variable, the proposed schemes are almost free of ray effects. Moreover, the above-mentioned way of imposing the positivity would not destroy both AP and second-order accuracy properties. To our best knowledge, this is the first time that spatial second-order, positive, asymptotic preserving and almost free of ray effects schemes are constructed for the nonlinear radiative transfer equations without operator splitting. Therefore, this paper improves our previous work on the first-order scheme [39] which could not be directly extended to high order, while keeping the solution positive. Various numerical experiments are included to validate the properties of the proposed schemes.

Keywords: Nonlinear gray radiative transfer equations, unified gas kinetic scheme, spatial second-order accuracy, positive preserving, asymptotic preserving, ray effects
MSC2010: 65-02, 65M08, 65M12, 35Q79, 85A02, 80M35

1 Introduction

The numerical simulation of the radiative transfer equations has a wide spectrum of applications in science and technology, such as in astrophysics and inertial confinement fusion research. From the view point of numerical simulation, the radiative transfer equations result in several difficulties, for example, the integro-differential form and high-dimensionality (time, spatial and angular variables). In particular, the multi-scale features characterized by wide-ranging optical thickness of background materials induce in numerical challenges. Indeed, the optical thickness of background materials has a great impact on the behavior of radiation transfer. For a material with low opacity, the radiation propagates in a transparent way, while for a material with high opacity, the radiation behaves like a diffusion process. In order to resolve the kinetic-scale-based radiative transfer equations in numerical simulation, the spatial mesh size in many numerical methods usually should be comparable to the photon's mean-free path, which is very small in the optically thick regions, leading to huge computational costs.

The other numerical challenges include preserving positivity and eliminating ray-effects. Namely, the positivity of the exact solution to the radiation transfer equations (i.e., the radiation intensity and the material temperature) should be preserved numerically. The appearance of negative numerical solution may cause the breakdown or instability of the numerical simulation. The ray effects caused by the usual discrete ordinate (S_N) method would destroy the symmetry when it is used to solve problems involving isolated sources within optically thin media.

In the recent years, the numerical simulation of the radiative transfer equations has been developed rapidly. An efficient approach to cope with the above-mentioned difficulties is the multi-scale numerical scheme that is asymptotic preserving (AP), positive preserving (PP) and free of or less susceptible to ray effects, whose construction remains a challenging issue even now. In fact, the schemes with AP property alone have been studied extensively in the literature [8, 16, 18, 19, 27, 36], including micro-macro decomposition, even-odd decomposition, implicit-explicit (IMEX) method and so on. There are also numerical schemes only focusing on the positive preserving property, such as in [5, 22, 24, 35, 41], the positive solution can be obtained through using a linear scaling limiter, or a flux limiter, or adopting special function spaces, etc. On the other hand, in order to mitigate the ray effects of the S_N method, alternative angular discretization methods, such as the angular finite element method[2, 4], wavelets method[3], angular adaptivity method[11, 34], spherical harmonic (P_N) method[1] have been proposed. Besides, the numerical schemes developed in [12, 15, 40] are both asymptotic preserving and positive preserving, while the

schemes in [20, 22] are positive and ray effects free as well.

The original unified gas kinetic scheme (UGKS) for continuum and rarefied flows in [37], which has been adopted to the linear radiation equation [27] and then extended to the nonlinear (frequency-dependent) radiative transfer equations ([29, 30, 31, 32, 33]), is proved to be asymptotic preserving. Numerical results, however, show that it is not positive preserving. Moreover, the aforementioned UGKS may suffer from ray effects, as it is based on the S_N method for the angular variable discretization. In order to mitigate the ray effects, we have extended the angular S_N method to the angular finite element and the filtered spherical harmonics (FP_N) approximation in our previous works [38, 39]. Due to the rotational invariance of the FP_N method, the scheme in [39] is almost free of ray effects. Remind that although the filtering technique [26, 28] can suppress spurious oscillations in the P_N approximation, the negative solution of the P_N approximation [25] may still occur. Thus, we have studied the PP property in [39] as well. Different from the positive FP_N schemes in [20, 22] where the PP property was achieved by imposing a positivity limiter, or by a positive moment closure that needs solving an additional expensive optimization problem, the PP property in [39] is obtained by giving the sufficient conditions to guarantee the positivity of the radiative energy density and material temperature, while the sufficient conditions are enforced through a much cheap linear scaling limiter. As far as we know, the scheme in [39] is almost the only one that possesses all the mentioned properties for the nonlinear radiative transfer equations; but unfortunately, the accuracy in the spatial variable is only of first order. We remark that the scheme in [21] also possesses all the above desired properties, but is for the linear radiative transfer equation. To obtain the PP property with spatial second-order accuracy, the authors in [40] constructed both PP and AP-UGKS schemes for *linear* radiation transfer equation only, based on the framework of UGKS and the angular S_N method, thus suffering from the ray effects.

In this paper, we shall extend our previous PP and AP FP_N -based UGKS for the nonlinear gray radiative transfer equations [39] from spatial first-order accuracy to the second-order. Compared with the linear radiative transfer equation in [40], for the case of the nonlinear gray radiative transfer equations, in order to achieve all the desired properties, particularly the positive preserving property, the extension is not trivial, and some additional techniques have to be introduced, for example, firstly, the linearized method of the implicit Monte Carlo (IMC) [6] is used here to construct the numerical boundary fluxes. Then, due to the requirement of piecewise linear reconstruction to get the spatial second-order accuracy, which brings technical difficulties in finding the sufficient conditions to preserve the positivity of the numerical solutions. Such difficulties have to be carefully dealt with. Finally, to make the positivity preserving conditions hold, we apply an additional linear scaling limiter to modify the reconstructed slopes, while for the first-order scheme in [39], such a limiter is not needed.

As in [40], by a detailed analysis of the numerical boundary fluxes, a simplification method of the fluxes in regimes $\epsilon \ll 1$ and $\epsilon = O(1)$ is presented to minimize the compu-

tational costs but without sacrificing the second-order accuracy. To our best knowledge, there seems no scheme for the nonlinear radiative transfer equations without operator splitting in the literature that is of spatial second-order accuracy, positive and asymptotic preserving, and almost free of ray effects.

The remainder of this paper is organized as follows. In Section 2 we introduce the nonlinear gray radiative transfer equations, while in Section 3 we present the construction of a spatial second-order FP_N -based UGKS. Through a detailed analysis in Section 4, we find the sufficient conditions to preserve the positivity of the FP_N -based UGKS and impose these conditions by using linear scaling limiters to obtain the positive UGKS. We then analyze the asymptotic preserving property of this positive scheme, and consequently, a positive and asymptotic preserving filtered spherical harmonics method ($PPFP_N$ -based UGKS) is hence proposed in this paper. In Section 5, we show that in the regime $\epsilon \ll 1$ and the regime $\epsilon = O(1)$, the boundary fluxes can be simplified. Therefore, a simplified $PPFP_N$ -based UGKS ($PPFP_N$ -based SUGKS) is obtained in these regimes. Section 6 presents a number of numerical tests to validate the current schemes. Finally, a conclusion is given in Section 7.

2 Model problems

We consider the following nonlinear radiative transfer equations, which are given in the scaled form:

$$\begin{cases} \frac{\epsilon^2}{c} \frac{\partial I}{\partial t} + \epsilon \mathbf{\Omega} \cdot \nabla_{\mathbf{r}} I = \sigma \left(\frac{1}{4\pi} acT^4 - I \right), \\ \epsilon^2 C_\nu \frac{\partial T}{\partial t} = \sigma \left(\int_{S^2} I d\mathbf{\Omega} - acT^4 \right). \end{cases} \quad (2.1)$$

The equations describe the radiative transfer and the energy exchange between radiation and background materials. Here \mathbf{r} denotes the scaled space variable (x, y, z) in \mathbb{R}^3 , t is the scaled time variable, $\mathbf{\Omega}$ is the angular variable (ξ, η, ζ) in S^2 (the unit sphere in \mathbb{R}^3). Functions $I(\mathbf{r}, \mathbf{\Omega}, t)$ and $T(\mathbf{r}, t)$ are the radiation intensity and material temperature, respectively. $\sigma(\mathbf{r}, T)$ is the scaled opacity, the radiation constant a and speed of light c also are scaled, $\epsilon > 0$ is the Knudsen number, and $C_\nu(\mathbf{r}, t)$ is the scaled heat capacity.

Equations (2.1) are a relaxation model for the radiation intensity to the local thermodynamic equilibrium, in which the emission source is a Planckian at local material temperature. It has been shown in [17] that as the parameter $\epsilon \rightarrow 0$, away from boundaries and initial layers, the intensity I approaches to a Planckian at local temperature T^0 , with T^0 satisfies a nonlinear diffusion equation, i.e.,

$$C_\nu \frac{\partial}{\partial t} T^{(0)} + a \frac{\partial}{\partial t} (T^{(0)})^4 = \nabla_{\mathbf{r}} \cdot \frac{ac}{3\sigma} \nabla_{\mathbf{r}} (T^{(0)})^4, \quad I^{(0)} = \frac{1}{4\pi} ac(T^{(0)})^4. \quad (2.2)$$

In the following, we denote $\phi = acT^4$, and rewrite (2.1) as

$$\begin{cases} \frac{\epsilon^2}{c} \frac{\partial I}{\partial t} + \epsilon \boldsymbol{\Omega} \cdot \nabla_{\mathbf{r}} I = \sigma \left(\frac{1}{4\pi} \phi - I \right), \\ \epsilon^2 \frac{\partial \phi}{\partial t} = \beta \sigma \left(\int_{S^2} I d\boldsymbol{\Omega} - \phi \right), \end{cases} \quad (2.3)$$

where $\beta \equiv \beta(x, t) = 4acT^3/C_\nu$.

3 A spatial second-order FP_N -based UGKS

In this section, we first revisit the filtered spherical harmonics (FP_N) discretization for the angular variable, and unified gas kinetic scheme (UGKS) for the spatial and temporal variables in [39]. And then, the construction of the spatial second-order fluxes is introduced in details, which is the crucial step to get the final positive preserving scheme. As a consequence, a spatial second-order FP_N -based UGKS is constructed for the equations (2.3).

3.1 Discretization of the angular, spatial and temporal variables

Denote by $\psi_\ell^m(\boldsymbol{\Omega})$ ($\ell \geq 0, -\ell \leq m \leq \ell$) the real normalized spherical harmonic function of degree ℓ and order m that satisfies $\langle \psi_\ell^m \psi_{\ell'}^{m'} \rangle = \delta_{\ell, \ell'} \delta_{m, m'}$, with $\langle \cdot \rangle = \int_{S^2} \cdot d\boldsymbol{\Omega}$ and $\delta_{\ell, \ell'}$ the Kronecker delta function. For any nonnegative integer N , let

$$\vec{\psi} = (\psi_0^0, \check{\psi}')', \quad \vec{I} = (I_0^0, \check{I}')',$$

with $\check{\psi} = (\psi_1^{-1}, \psi_1^0, \psi_1^1, \dots, \psi_N^N)'$ the spherical harmonic vector and $I_0^0 = \langle \psi_0^0 I \rangle$, $\check{I} = \langle \check{\psi} I \rangle$ the corresponding moments, here the upper script $'$ is the transpose operation. Moreover, denoting $\rho = \int_{S^2} I d\boldsymbol{\Omega}$ and noting that $I_0^0 = \frac{1}{2\sqrt{\pi}} \rho$, one has

$$\vec{I} = \left(\frac{1}{2\sqrt{\pi}} \rho, \check{I}' \right)'. \quad (3.1)$$

With the FP_N angular discretization and macro-micro decomposition as in [39], we can obtain

$$\begin{cases} \frac{\epsilon^2}{c} \frac{\partial \rho}{\partial t} + \epsilon \nabla_{\mathbf{r}} \cdot \langle \boldsymbol{\Omega} I \rangle = \sigma(\phi - \rho), \\ \epsilon^2 \frac{\partial \phi}{\partial t} = \beta \sigma(\rho - \phi), \end{cases} \quad (3.2)$$

and

$$\frac{\epsilon^2}{c} \frac{\partial \check{I}}{\partial t} + \epsilon \nabla_{\mathbf{r}} \cdot \langle \check{\psi} \boldsymbol{\Omega} I \rangle = -\sigma \check{I} - \frac{\epsilon^2}{c} \sigma_f \check{\mathbf{F}} \check{I}, \quad (3.3)$$

which are referred to as the macro and micro equations, respectively. Here $\nabla_{\mathbf{r}} \cdot \langle \check{\psi} \boldsymbol{\Omega} I \rangle = \partial_x \langle \check{\psi} \xi I \rangle + \partial_y \langle \check{\psi} \eta I \rangle + \partial_z \langle \check{\psi} \zeta I \rangle$. $\sigma_f \geq 0$ is a filter parameter, $\check{\mathbf{F}}$ is a diagonal filtering matrix with elements $\check{\mathbf{F}}_{(\ell, m), (\ell, m)} = -\ln(f(\frac{\ell}{N+1}))$, and $f: \mathbb{R}^+ \rightarrow [0, 1]$ is a filter function with $f(0) = 1$.

To discretize the spatial and temporal variables of (3.2)-(3.3), similar to that in [39], only the two-dimensional Cartesian spatial case is considered. Therefore, one has $\mathbf{r} = (x, y)$, $\mathbf{\Omega} = (\xi, \eta)$ and $\nabla_{\mathbf{r}} \cdot \langle \vec{\psi} \mathbf{\Omega} I \rangle = \partial_x \langle \vec{\psi} \xi I \rangle + \partial_y \langle \vec{\psi} \eta I \rangle$ in the 2-D setting. And also a uniform partition of the space and time variables is considered for simplicity. Denote by $\Delta x, \Delta y, \Delta t$ the mesh sizes and by x_i, y_j, t_n ($i, j, n \in \mathbb{Z}$) the corresponding mesh nodes. Let (i, j) be the cell $\{(x, y) : x_{i-1/2} < x < x_{i+1/2}, y_{j-1/2} < y < y_{j+1/2}\}$ with $x_{i\pm 1/2} = (x_i + x_{i\pm 1})/2$, $y_{j\pm 1/2} = (y_j + y_{j\pm 1})/2$ being the cell interfaces of (i, j) . For any function $\varphi(x, y, t)$, denote

$$\varphi_{i,j}^n = \frac{1}{\Delta x \Delta y} \int_{y_{j-\frac{1}{2}}}^{y_{j+\frac{1}{2}}} \int_{x_{i-\frac{1}{2}}}^{x_{i+\frac{1}{2}}} \varphi(x, y, t_n) dx dy.$$

Then, from [39], one has the following conservative finite volume scheme:

$$\begin{cases} \rho_{i,j}^{n+1} = \rho_{i,j}^n + \frac{\Delta t}{\Delta x} \left(\Phi_{i-1/2,j}^{n+1} - \Phi_{i+1/2,j}^{n+1} \right) + \frac{\Delta t}{\Delta y} \left(\Upsilon_{i,j-1/2}^{n+1} - \Upsilon_{i,j+1/2}^{n+1} \right) \\ \quad + \frac{\sigma_{i,j}^{n+1} c \Delta t}{\epsilon^2} (\phi_{i,j}^{n+1} - \rho_{i,j}^{n+1}), \\ \phi_{i,j}^{n+1} = \phi_{i,j}^n + \frac{\beta_{i,j}^{n+1} \sigma_{i,j}^{n+1} \Delta t}{\epsilon^2} \left(\rho_{i,j}^{n+1} - \phi_{i,j}^{n+1} \right), \end{cases} \quad (3.4)$$

and

$$\begin{aligned} \check{\mathbf{I}}_{i,j}^{n+1} &= \check{\mathbf{I}}_{i,j}^n + \frac{\Delta t}{\Delta x} \left(\vec{\mathbf{G}}_{i-1/2,j} - \vec{\mathbf{G}}_{i+1/2,j} \right) + \frac{\Delta t}{\Delta y} \left(\vec{\mathbf{H}}_{i,j-1/2} - \vec{\mathbf{H}}_{i,j+1/2} \right) \\ &\quad - \frac{\sigma_{i,j}^{n+1} c \Delta t}{\epsilon^2} \check{\mathbf{I}}_{i,j}^{n+1} - \Delta t \sigma_f \check{\mathbf{F}} \check{\mathbf{I}}_{i,j}^{n+1}, \end{aligned} \quad (3.5)$$

where the interface fluxes are given by

$$\begin{aligned} \Phi_{i-1/2,j}^{n+1} &= \frac{c}{\epsilon \Delta t} \int_{t_n}^{t_{n+1}} \langle \xi I(x_{i-\frac{1}{2}}, y_j, \mathbf{\Omega}, t) \rangle dt, \quad \vec{\mathbf{G}}_{i-1/2,j} = \frac{c}{\epsilon \Delta t} \int_{t_n}^{t_{n+1}} \langle \xi \check{\psi} I(x_{i-\frac{1}{2}}, y_j, \mathbf{\Omega}, t) \rangle dt, \\ \Upsilon_{i,j-1/2}^{n+1} &= \frac{c}{\epsilon \Delta t} \int_{t_n}^{t_{n+1}} \langle \eta I(x_i, y_{j-\frac{1}{2}}, \mathbf{\Omega}, t) \rangle dt, \quad \vec{\mathbf{H}}_{i,j-1/2} = \frac{c}{\epsilon \Delta t} \int_{t_n}^{t_{n+1}} \langle \eta \check{\psi} I(x_i, y_{j-\frac{1}{2}}, \mathbf{\Omega}, t) \rangle dt, \end{aligned} \quad (3.6)$$

and will be determined in the next subsection so as to update the system (3.4)-(3.5).

3.2 Method for the fluxes' construction

This subsection is devoted to constructing the interface fluxes $\Phi_{i-1/2,j}^{n+1}$, $\Upsilon_{i-1/2,j}^{n+1}$ and $\vec{\mathbf{G}}_{i-1/2,j}$, $\vec{\mathbf{H}}_{i,j-1/2}$ in (3.6). In order to get a positive-preserving scheme, the construction of the fluxes here is slightly different from that in [39].

As done in the IMC scheme [6], we discretize the time variable of the second equation of (2.3) firstly, and obtain

$$\epsilon^2 \frac{\phi^{n+1} - \phi^n}{\Delta t} = \beta^{n+1} \sigma^{n+1} \left(\rho^{n+1} - \phi^{n+1} \right),$$

which implies

$$\begin{aligned} \phi^{n+1} &= \frac{\epsilon^2}{\epsilon^2 + \Delta t (\beta \sigma)^{n+1}} \phi^n + \frac{\Delta t (\beta \sigma)^{n+1}}{\epsilon^2 + \Delta t (\beta \sigma)^{n+1}} \rho^{n+1} \\ &\equiv \kappa^{n+1} \phi^n + (1 - \kappa^{n+1}) \rho^{n+1}, \end{aligned} \quad (3.7)$$

where $\kappa = \frac{\epsilon^2}{\epsilon^2 + \Delta t \beta \sigma}$. Replacing ϕ by ϕ^{n+1} in the first equation of (2.3), we substitute (3.7) into it to arrive at

$$\frac{\epsilon^2}{c} \frac{\partial I}{\partial t} + \epsilon \mathbf{\Omega} \cdot \nabla_{\mathbf{r}} I = \sigma \left(\frac{1}{4\pi} (\kappa^{n+1} \phi^n + (1 - \kappa^{n+1}) \rho^{n+1}) - I \right). \quad (3.8)$$

In order to get the x -direction numerical fluxes $\Phi_{i-1/2,j}^{n+1}$ and $\vec{\mathbf{G}}_{i-1/2,j}$, we consider the solution of the following initial value problem at cell interface $x = x_{i-1/2}, y = y_j$:

$$\begin{cases} \frac{\epsilon}{c} \frac{\partial I}{\partial t} + \xi \frac{\partial I}{\partial x} = \frac{\sigma_{i-1/2,j}^{n+1}}{\epsilon} \left(\frac{1}{4\pi} (\kappa^{n+1} \phi^n + (1 - \kappa_{i-1/2,j}^{n+1}) \rho^{n+1}) - I \right), \\ I(x, y_j, \mathbf{\Omega}, t)|_{t=t_n} = I^0(x, y_j, \mathbf{\Omega}), \end{cases} \quad (3.9)$$

where $\sigma_{i-1/2,j}^{n+1}, \kappa_{i-1/2,j}^{n+1}$ are supposed to be approximate constants of σ, κ around t_{n+1} at the corresponding cell interface. Then, the time-dependent solution of (3.9) can be written as

$$\begin{aligned} & I(x_{i-1/2}, y_j, \mathbf{\Omega}, t) \\ &= e^{-\nu_{i-1/2,j}^{n+1}(t-t_n)} I^0 \left(x_{i-1/2} - \frac{c\xi}{\epsilon}(t-t_n), y_j, \mathbf{\Omega} \right) \\ &+ \frac{\nu_{i-1/2,j}^{n+1}}{4\pi} \int_{t_n}^t e^{-\nu_{i-1/2,j}^{n+1}(t-s)} \left(\kappa^{n+1} \phi^n + (1 - \kappa_{i-1/2,j}^{n+1}) \rho^{n+1} \right) \left(x_{i-1/2} - \frac{c\xi}{\epsilon}(t-s), y_j \right) ds, \end{aligned} \quad (3.10)$$

where $\nu = c\sigma/\epsilon^2$.

Now, in order to fully determine the solution in (3.10), it remains to give approximations of the initial data $I^0(x, y_j, \mathbf{\Omega})$, $(\kappa^{n+1} \phi^n)(x, y_j)$ and $\rho^{n+1}(x, y_j)$ around the cell interface $(x_{i-1/2}, y_j)$. In UGKS, they are obtained through polynomial reconstructions. Here, we use the following piecewise linear reconstructions:

$$I^0(x, y_j, \mathbf{\Omega}) = \vec{\psi} \cdot (\vec{\mathbf{I}}_{i,j}^n + \delta_x \vec{\mathbf{I}}_{i,j}^n(x - x_i)), \quad x \in (x_{i-1/2}, x_{i+1/2}), \quad (3.11)$$

$$(k^{n+1} \phi^n)(x, y_j) = (\kappa^{n+1} \phi^n)_{i-1/2,j} + \delta_x (\kappa^{n+1} \phi^n)_{i-1/2,j}(x - x_{i-1/2}), \quad x \in (x_{i-1}, x_i), \quad (3.12)$$

$$\rho^{n+1}(x, y_j) = \rho_{i-1/2,j}^{n+1} + \delta_x \rho_{i-1/2,j}^{n+1}(x - x_{i-1/2}), \quad x \in (x_{i-1}, x_i), \quad (3.13)$$

where $\delta_x \vec{\mathbf{I}} = (\delta_x I_0^0, \delta_x I_1^{-1}, \dots, \delta_x I_N^N)'$ are the slopes, and the second order MUSCL slope limiter is used to remove (possible) spurious oscillations. And $\varphi_{i-1/2,j}, \delta_x \varphi_{i-1/2,j}$ (for $\varphi = \kappa^{n+1} \phi^n$ or ρ^{n+1}) are the cell interface value and the finite difference approximation respectively, which are given by

$$\varphi_{i-1/2,j} = \frac{\varphi_{i,j} + \varphi_{i-1,j}}{2}, \quad \delta_x \varphi_{i-1/2,j} = \frac{\varphi_{i,j} - \varphi_{i-1,j}}{\Delta x}.$$

We remark here that since the piecewise linear reconstructions have been used for the spatial variable, the scheme is of second-order accuracy in space. We shall verify the spatial second-order accuracy numerically in Section 6.

Substituting (3.11)-(3.13) into (3.10), we obtain the approximation formula of the interface intensity $I(x_{i-1/2}, y_j, \mathbf{\Omega}, t)$ that depends on the macro quantities ρ and ϕ .

With the above obtained approximation of $I(x_{i-1/2}, y_j, \mathbf{\Omega}, t)$ in (3.10), the expressions for the numerical fluxes $\Phi_{i-1/2,j}^{n+1}$ and $\vec{G}_{i-1/2,j}$ can be computed, which are

$$\begin{aligned}\Phi_{i-1/2,j}^{n+1} &= \frac{c}{\epsilon \Delta t} \int_{t_n}^{t_{n+1}} \langle \xi I(x_{i-\frac{1}{2}}, y_j, \mathbf{\Omega}, t) \rangle dt \\ &= \tilde{\alpha}_{i-1/2,j}^{n+1} \left\{ \langle \xi \vec{\psi} \rangle_{1,4} \cdot \left(\vec{I}_{i-1,j}^n + \frac{\Delta x}{2} \delta_x \vec{I}_{i-1,j}^n \right) + \langle \xi \vec{\psi} \rangle_{2,3} \cdot \left(\vec{I}_{i,j}^n - \frac{\Delta x}{2} \delta_x \vec{I}_{i,j}^n \right) \right\} \\ &\quad + \tilde{b}_{i-1/2,j}^{n+1} \left(\langle \xi^2 \vec{\psi} \rangle_{1,4} \cdot \delta_x \vec{I}_{i-1,j}^n + \langle \xi^2 \vec{\psi} \rangle_{2,3} \cdot \delta_x \vec{I}_{i,j}^n \right) \\ &\quad + \tilde{d}_{i-1/2,j}^{n+1} \frac{4\pi}{3} \left(\delta_x (\kappa^{n+1} \phi^n)_{i-1/2,j} + (1 - \kappa_{i-1/2,j}^{n+1}) \delta_x \rho_{i-1/2,j}^{n+1} \right),\end{aligned}\quad (3.14)$$

$$\begin{aligned}\vec{G}_{i-1/2,j} &= \frac{c}{\epsilon \Delta t} \int_{t_n}^{t_{n+1}} \langle \xi \check{\vec{\psi}} I(x_{i-\frac{1}{2}}, y_j, \mathbf{\Omega}, t) \rangle dt \\ &= \tilde{\alpha}_{i-1/2,j}^{n+1} \left\{ \langle \xi \check{\vec{\psi}} \vec{\psi}' \rangle_{1,4} \cdot \left(\vec{I}_{i-1,j}^n + \frac{\Delta x}{2} \delta_x \vec{I}_{i-1,j}^n \right) + \langle \xi \check{\vec{\psi}} \vec{\psi}' \rangle_{2,3} \cdot \left(\vec{I}_{i,j}^n - \frac{\Delta x}{2} \delta_x \vec{I}_{i,j}^n \right) \right\} \\ &\quad + \tilde{b}_{i-1/2,j}^{n+1} \left(\langle \xi^2 \check{\vec{\psi}} \vec{\psi}' \rangle_{1,4} \cdot \delta_x \vec{I}_{i-1,j}^n + \langle \xi^2 \check{\vec{\psi}} \vec{\psi}' \rangle_{2,3} \cdot \delta_x \vec{I}_{i,j}^n \right) \\ &\quad + \tilde{c}_{i-1/2,j}^{n+1} \langle \xi \check{\vec{\psi}} \rangle \left((\kappa^{n+1} \phi^n)_{i-1/2,j} + (1 - \kappa_{i-1/2,j}^{n+1}) \rho_{i-1/2,j}^{n+1} \right) \\ &\quad + \tilde{d}_{i-1/2,j}^{n+1} \langle \xi^2 \check{\vec{\psi}} \rangle \left(\delta_x (\kappa^{n+1} \phi^n)_{i-1/2,j} + (1 - \kappa_{i-1/2,j}^{n+1}) \delta_x \rho_{i-1/2,j}^{n+1} \right),\end{aligned}\quad (3.15)$$

where the coefficients $\tilde{\alpha}_{i-1/2,j}^{n+1}$, $\tilde{b}_{i-1/2,j}^{n+1}$, $\tilde{c}_{i-1/2,j}^{n+1}$, $\tilde{d}_{i-1/2,j}^{n+1}$ are given by

$$\begin{aligned}\tilde{\alpha}(\Delta t, \epsilon, \sigma) &= \frac{c}{\epsilon \Delta t \nu} (1 - e^{-\nu \Delta t}), \\ \tilde{b}(\Delta t, \epsilon, \sigma) &= -\frac{c^2}{\epsilon^2 \nu^2 \Delta t} (1 - e^{-\nu \Delta t} - \nu \Delta t e^{-\nu \Delta t}), \\ \tilde{c}(\Delta t, \epsilon, \sigma) &= \frac{c^2 \sigma}{4\pi \Delta t \epsilon^3 \nu} \left(\Delta t - \frac{1}{\nu} (1 - e^{-\nu \Delta t}) \right), \\ \tilde{d}(\Delta t, \epsilon, \sigma) &= -\frac{c^3 \sigma}{4\pi \Delta t \epsilon^4 \nu^2} \left(\Delta t (1 + e^{-\nu \Delta t}) - \frac{2}{\nu} (1 - e^{-\nu \Delta t}) \right),\end{aligned}\quad (3.16)$$

with $\sigma_{i-1/2,j}^{n+1} = \frac{2\sigma_{i,j}^{n+1}\sigma_{i-1,j}^{n+1}}{\sigma_{i,j}^{n+1} + \sigma_{i-1,j}^{n+1}}$ on the boundary. And $\langle \cdot \rangle_{1,4}$ denotes the angular integration over the $\xi > 0$ region of the unit sphere, while $\langle \cdot \rangle_{2,3}$ over the $\xi < 0$ region.

Similarly, the y -direction fluxes $\Upsilon_{i,j-1/2}^{n+1}$ and $\vec{H}_{i,j-1/2}$ can be constructed, and take the following form:

$$\begin{aligned}\Upsilon_{i,j-1/2}^{n+1} &= \tilde{\alpha}_{i,j-1/2}^{n+1} \left\{ \langle \eta \vec{\psi} \rangle_{1,2} \cdot \left(\vec{I}_{i,j-1}^n + \frac{\Delta y}{2} \delta_y \vec{I}_{i,j-1}^n \right) + \langle \eta \vec{\psi} \rangle_{3,4} \cdot \left(\vec{I}_{i,j}^n - \frac{\Delta y}{2} \delta_y \vec{I}_{i,j}^n \right) \right\} \\ &\quad + \tilde{b}_{i,j-1/2}^{n+1} \left(\langle \eta^2 \vec{\psi} \rangle_{1,2} \cdot \delta_y \vec{I}_{i,j-1}^n + \langle \eta^2 \vec{\psi} \rangle_{3,4} \cdot \delta_y \vec{I}_{i,j}^n \right) \\ &\quad + \tilde{d}_{i,j-1/2}^{n+1} \frac{4\pi}{3} \left(\delta_y (\kappa^{n+1} \phi^n)_{i,j-1/2} + (1 - \kappa_{i,j-1/2}^{n+1}) \delta_y \rho_{i,j-1/2}^{n+1} \right),\end{aligned}\quad (3.17)$$

$$\begin{aligned}
\vec{\mathbf{H}}_{i,j-1/2} = & \tilde{\alpha}_{i,j-1/2}^{n+1} \left\{ \langle \eta \vec{\psi} \vec{\psi}' \rangle_{1,2} \cdot \left(\vec{\mathbf{I}}_{i,j-1}^n + \frac{\Delta y}{2} \delta_y \vec{\mathbf{I}}_{i,j-1}^n \right) + \langle \eta \vec{\psi} \vec{\psi}' \rangle_{3,4} \cdot \left(\vec{\mathbf{I}}_{i,j}^n - \frac{\Delta y}{2} \delta_y \vec{\mathbf{I}}_{i,j}^n \right) \right\} \\
& + \tilde{b}_{i,j-1/2}^{n+1} \left(\langle \eta^2 \vec{\psi} \vec{\psi}' \rangle_{1,2} \cdot \delta_y \vec{\mathbf{I}}_{i,j-1}^n + \langle \eta^2 \vec{\psi} \vec{\psi}' \rangle_{3,4} \cdot \delta_y \vec{\mathbf{I}}_{i,j}^n \right) \\
& + \tilde{c}_{i,j-1/2}^{n+1} \langle \eta \vec{\psi} \rangle \left((k^{n+1} \phi^n)_{i,j-1/2} + (1 - k_{i,j-1/2}^{n+1}) \rho_{i,j-1/2}^{n+1} \right) \\
& + \tilde{d}_{i,j-1/2}^{n+1} \langle \eta^2 \vec{\psi} \rangle \left(\delta_y (\kappa^{n+1} \phi^n)_{i,j-1/2} + (1 - \kappa_{i,j-1/2}^{n+1}) \delta_y \rho_{i,j-1/2}^{n+1} \right), \tag{3.18}
\end{aligned}$$

where for $\varphi = \kappa^{n+1} \phi^n$ or ρ^{n+1} , $\varphi_{i,j-1/2} = \frac{\varphi_{i,j} + \varphi_{i,j-1}}{2}$, $\delta_y \varphi_{i,j-1/2} = \frac{\varphi_{i,j} - \varphi_{i,j-1}}{\Delta y}$, $\sigma_{i,j-1/2}^{n+1} = \frac{2\sigma_{i,j}^{n+1} \sigma_{i,j-1}^{n+1}}{\sigma_{i,j}^{n+1} + \sigma_{i,j-1}^{n+1}}$. And $\langle \cdot \rangle_{1,2}$ denotes the angular integration over the $\eta > 0$ region of the unit sphere, while $\langle \cdot \rangle_{3,4}$ over the $\eta < 0$ region.

Up to now, we have completed the construction of the numerical fluxes.

3.3 FP_N -based UGKS for (2.3)

With the numerical fluxes in hand, we summarize the whole procedure of the currently constructed FP_N -based UGKS in the following.

We note that the nonlinear macro equations (3.4) can be solved by the iteration method used in [29, 39]. Moreover, substituting (3.7) into the first equation of (3.4), we can obtain the decoupled iterative macro system. Now, we state it in the following:

Loop of the FP_N -based UGKS: Given $\vec{\mathbf{I}}_{i,j}^n$, $T_{i,j}^n$, one has $\rho_{i,j}^n$ and $\vec{\mathbf{I}}_{i,j}^n$. Find $\vec{\mathbf{I}}_{i,j}^{n+1}$ (i.e., $\rho_{i,j}^{n+1}$, $\vec{\mathbf{I}}_{i,j}^{n+1}$) and $T_{i,j}^{n+1}$.

1) Solve the nonlinear macro equations (3.4) by the following iteration method to get $\rho_{i,j}^{n+1}$, $T_{i,j}^{n+1}$:

1.1) Set the initial iteration values $\rho_{i,j}^{n+1,0}$, $T_{i,j}^{n+1,0}$ (e.g. take $\rho_{i,j}^{n+1,0} = \rho_{i,j}^n$, $T_{i,j}^{n+1,0} = T_{i,j}^n$);

1.2) For $s = 0, 1, \dots, S$,

Compute the coefficients $\sigma_{i,j}^{n+1,s}$, $\beta_{i,j}^{n+1,s}$, $\kappa_{i,j}^{n+1,s}$, $\tilde{\alpha}_{i-1/2,j}^{n+1,s}$, $\tilde{b}_{i-1/2,j}^{n+1,s}$, $\tilde{d}_{i-1/2,j}^{n+1,s}$ with the value of $T_{i,j}^{n+1,s}$, and solve the following linearized equation to get $\rho_{i,j}^{n+1,s+1}$

$$\begin{aligned}
\rho_{i,j}^{n+1,s+1} = & \rho_{i,j}^n + \frac{\Delta t}{\Delta x} \left(\Phi_{i-1/2,j}^{n+1,s+1} - \Phi_{i+1/2,j}^{n+1,s+1} \right) + \frac{\Delta t}{\Delta y} \left(\Upsilon_{i,j-1/2}^{n+1,s+1} - \Upsilon_{i,j+1/2}^{n+1,s+1} \right) \\
& + \frac{\sigma_{i,j}^{n+1,s} c \Delta t}{\epsilon^2} \kappa_{i,j}^{n+1,s} (\phi_{i,j}^n - \rho_{i,j}^{n+1,s+1}), \tag{3.19}
\end{aligned}$$

where

$$\begin{aligned}
\Phi_{i-1/2,j}^{n+1,s+1} = & \tilde{\alpha}_{i-1/2,j}^{n+1,s} \left\{ \langle \xi \vec{\psi} \rangle_{1,4} \cdot \left(\vec{\mathbf{I}}_{i-1,j}^n + \frac{\Delta x}{2} \delta_x \vec{\mathbf{I}}_{i-1,j}^n \right) + \langle \xi \vec{\psi} \rangle_{2,3} \cdot \left(\vec{\mathbf{I}}_{i,j}^n - \frac{\Delta x}{2} \delta_x \vec{\mathbf{I}}_{i,j}^n \right) \right\} \\
& + \tilde{b}_{i-1/2,j}^{n+1,s} \left(\langle \xi^2 \vec{\psi} \rangle_{1,4} \cdot \delta_x \vec{\mathbf{I}}_{i-1,j}^n + \langle \xi^2 \vec{\psi} \rangle_{2,3} \cdot \delta_x \vec{\mathbf{I}}_{i,j}^n \right) \\
& + \tilde{d}_{i-1/2,j}^{n+1,s} \frac{4\pi}{3} \left(\delta_x (\kappa^{n+1,s} \phi^n)_{i-1/2,j} + (1 - \kappa_{i-1/2,j}^{n+1,s}) \delta_x \rho_{i-1/2,j}^{n+1,s+1} \right),
\end{aligned}$$

and similarly for $\Upsilon_{i,j-1/2}^{n+1,s+1}$.

Substitute $\rho_{i,j}^{n+1,s+1}$ into the following equation to get $\phi_{i,j}^{n+1,s+1}$:

$$\phi_{i,j}^{n+1,s+1} = \kappa_{i,j}^{n+1,s} \phi_{i,j}^n + (1 - \kappa_{i,j}^{n+1,s}) \rho_{i,j}^{n+1,s+1}. \tag{3.20}$$

1.3) Calculate the iteration error, exit when convergence, and set

$$\rho_{i,j}^{n+1} = \rho_{i,j}^{n+1,s+1}, \quad \phi_{i,j}^{n+1} = \phi_{i,j}^{n+1,s+1}, \quad T_{i,j}^{n+1} = \left(\frac{\phi_{i,j}^{n+1}}{ac}\right)^{\frac{1}{4}}.$$

2) With the obtained $\rho_{i,j}^{n+1}$, $\phi_{i,j}^{n+1}$ and $T_{i,j}^{n+1}$, compute $\sigma_{i,j}^{n+1}$ and the fluxes $\vec{\mathbf{G}}_{i\pm 1/2,j}^{n+1}$, $\vec{\mathbf{H}}_{i,j\pm 1/2}^{n+1}$. Then, $\check{\mathbf{I}}_{i,j}^{n+1}$ can be obtained directly from the following linear micro equations:

$$\begin{aligned} \check{\mathbf{I}}_{i,j}^{n+1} = & \check{\mathbf{I}}_{i,j}^n + \frac{\Delta t}{\Delta x} \left(\vec{\mathbf{G}}_{i-1/2,j} - \vec{\mathbf{G}}_{i+1/2,j} \right) + \frac{\Delta t}{\Delta y} \left(\vec{\mathbf{H}}_{i,j-1/2} - \vec{\mathbf{H}}_{i,j+1/2} \right) \\ & - \frac{\sigma_{i,j}^{n+1} c \Delta t}{\epsilon^2} \check{\mathbf{I}}_{i,j}^{n+1} - \Delta t \sigma_f \check{\mathbf{F}} \check{\mathbf{I}}_{i,j}^{n+1}. \end{aligned}$$

3) Goto 1) for the next computational time step.

End

4 Analysis of the FP_N -based UGKS

This section is devoted to analyzing the fluxes in the above FP_N -based UGKS and making the scheme be both positive preserving and asymptotic preserving. First, in Subsection 4.1, by a detailed analysis of the linearized iteration equations (3.19)-(3.20), we can obtain the sufficient conditions that preserve the positivity of the macro auxiliary quantities $\rho_{i,j}^{n+1,s+1}$ and $\phi_{i,j}^{n+1,s+1}$ in every iteration. This implies the positivity of the radiation energy density $\rho_{i,j}^{n+1}$ and material temperature $T_{i,j}^{n+1}$. Then, in Subsection 4.2, linear scaling limiters, which are realizable, are given to enforce those sufficient conditions to hold. Finally, we analyze the asymptotic preserving property of the scheme in Subsection 4.3. Thus, the desired positive preserving and asymptotic preserving FP_N -based UGKS, called $PPFP_N$ -based UGKS, is obtained.

4.1 Positivity analysis

For convenience, we decompose the macro flux $\Phi_{i-1/2,j}^{n+1,s+1}$ into the following three parts:

$$\Phi_{i-1/2,j}^{n+1,s+1} = \Phi_{i-1/2,j}^{n+1,s+1}(\vec{\mathbf{I}}^n) + \Phi_{i-1/2,j}^{n+1,s+1}(\phi^n) + \Phi_{i-1/2,j}^{n+1,s+1}(\rho^{n+1,s+1}),$$

where $\Phi_{i-1/2,j}^{n+1,s+1}(\vec{\mathbf{I}}^n)$, $\Phi_{i-1/2,j}^{n+1,s+1}(\phi^n)$, $\Phi_{i-1/2,j}^{n+1,s+1}(\rho^{n+1,s+1})$ denote the terms that are related to $\vec{\mathbf{I}}^n$, ϕ^n and $\rho^{n+1,s+1}$ in the macro flux $\Phi_{i-1/2,j}^{n+1,s+1}$ of (3.19) respectively. And the other macro fluxes, such as $\Upsilon_{i,j-1/2}^{n+1,s+1}$, can be handled similarly. Next, we prove a sufficient condition that makes the solution of the linearized equations (3.19)-(3.20) positive. More precisely,

Theorem 4.1. *Given $\rho_{i,j}^n \geq 0$, $\phi_{i,j}^n \geq 0$ and $\phi_{i,j}^{n+1,s} \geq 0$. Suppose that Δt satisfies*

$$\Delta t \tilde{\alpha}^{n+1,s}(\Delta t, \epsilon, \sigma_{\min}) \leq \frac{\Delta x \Delta y}{2(\Delta x + \Delta y)}, \quad \max_{i,j} \left(-\frac{\tilde{d}_{i\pm 1/2,j\pm 1/2}^{n+1,s}(\Delta t)}{\sigma_{i,j}^{n+1,s}} \right) \leq \frac{3c(\Delta x \Delta y)^2}{8\pi\epsilon^2((\Delta x)^2 + (\Delta y)^2)}, \quad (4.1)$$

where $\sigma_{\min} = \min_{i,j} \sigma_{i,j}^{n+1,s}$. Furthermore, for any cell (i,j) , assume that the initial data $\vec{\mathbf{I}}_{i,j}^n = (\frac{1}{2\sqrt{\pi}}\rho_{i,j}^n, \check{\vec{\mathbf{I}}}_{i,j}^n)'$ satisfies

$$\begin{aligned} & \frac{1}{4} \left(\frac{\tilde{\alpha}_{i-1/2,j}^{n+1,s}}{\Delta x} + \frac{\tilde{\alpha}_{i+1/2,j}^{n+1,s}}{\Delta x} + \frac{\tilde{\alpha}_{i,j-1/2}^{n+1,s}}{\Delta y} + \frac{\tilde{\alpha}_{i,j+1/2}^{n+1,s}}{\Delta y} \right) \rho_{i,j}^n + \left\{ \frac{\tilde{\alpha}_{i-1/2,j}^{n+1,s}}{\Delta x} \langle \xi \check{\vec{\psi}} \rangle_{2,3} \right. \\ & \left. - \frac{\tilde{\alpha}_{i+1/2,j}^{n+1,s}}{\Delta x} \langle \xi \check{\vec{\psi}} \rangle_{1,4} + \frac{\tilde{\alpha}_{i,j-1/2}^{n+1,s}}{\Delta y} \langle \eta \check{\vec{\psi}} \rangle_{3,4} - \frac{\tilde{\alpha}_{i,j+1/2}^{n+1,s}}{\Delta y} \langle \eta \check{\vec{\psi}} \rangle_{1,2} \right\} \check{\vec{\mathbf{I}}}_{i,j}^n \geq 0, \end{aligned} \quad (4.2)$$

and

$$\begin{cases} \langle \xi \vec{\psi} \rangle_{1,4} \cdot \vec{\mathbf{I}}_{i,j}^n \pm \langle (\frac{\Delta x}{2} \xi + \frac{\tilde{b}_{i+1/2,j}^{n+1,s}}{\tilde{\alpha}_{i+1/2,j}^{n+1,s}} \xi^2) \vec{\psi} \rangle_{1,4} \cdot \delta_x \vec{\mathbf{I}}_{i,j}^n \geq 0, \\ \langle -\xi \vec{\psi} \rangle_{2,3} \cdot \vec{\mathbf{I}}_{i,j}^n \pm \langle (\frac{\Delta x}{2} \xi + \frac{\tilde{b}_{i-1/2,j}^{n+1,s}}{\tilde{\alpha}_{i-1/2,j}^{n+1,s}} \xi^2) \vec{\psi} \rangle_{2,3} \cdot \delta_x \vec{\mathbf{I}}_{i,j}^n \geq 0, \end{cases} \quad (4.3)$$

$$\begin{cases} \langle \eta \vec{\psi} \rangle_{1,2} \cdot \vec{\mathbf{I}}_{i,j}^n \pm \langle (\frac{\Delta y}{2} \eta + \frac{\tilde{b}_{i,j+1/2}^{n+1,s}}{\tilde{\alpha}_{i,j+1/2}^{n+1,s}} \eta^2) \vec{\psi} \rangle_{1,2} \cdot \delta_y \vec{\mathbf{I}}_{i,j}^n \geq 0, \\ \langle -\eta \vec{\psi} \rangle_{3,4} \cdot \vec{\mathbf{I}}_{i,j}^n \pm \langle (\frac{\Delta y}{2} \eta + \frac{\tilde{b}_{i,j-1/2}^{n+1,s}}{\tilde{\alpha}_{i,j-1/2}^{n+1,s}} \eta^2) \vec{\psi} \rangle_{3,4} \cdot \delta_y \vec{\mathbf{I}}_{i,j}^n \geq 0. \end{cases} \quad (4.4)$$

Then, it holds that

$$\rho_{i,j}^{n+1,s+1} \geq 0, \quad \phi_{i,j}^{n+1,s+1} \geq 0.$$

Proof. We first give the proof of $\rho_{i,j}^{n+1,s+1} \geq 0$. Once it is obtained, by (3.20) and the condition $\phi_{i,j}^n \geq 0$, and the fact $\kappa = \frac{\epsilon^2}{\epsilon^2 + \Delta t \beta \sigma} \in [0, 1]$, we obtain $\phi_{i,j}^{n+1,s+1} \geq 0$ immediately.

Denote by

$$\vec{\rho}^{s+1} = (\rho_{1,1}^{n+1,s+1}, \rho_{1,2}^{n+1,s+1}, \dots, \rho_{2,1}^{n+1,s+1}, \rho_{2,2}^{n+1,s+1}, \dots)'$$

the solution of the discrete linearized macro equation (3.19). Thus we can rewrite equation (3.19) into the following matrix form

$$\mathbf{A}^s \vec{\rho}^{s+1} = \vec{\mathbf{b}}^s.$$

Here \mathbf{A}^s is the coefficient matrix of (3.19) and $\vec{\mathbf{b}}^s$ denotes the right-hand term. For the matrix \mathbf{A}^s , one sees that for any $\Delta t > 0$, $\epsilon \geq 0$, $\sigma \geq 0$, the coefficient function $\tilde{d}(\Delta t, \epsilon, \sigma) \leq 0$ and $0 \leq \kappa \leq 1$. Then, one easily verifies that

$$\mathbf{A}^s(p, q) \leq 0 \quad \forall p \neq q, \quad \text{and} \quad \sum_q \mathbf{A}^s(p, q) > 0 \quad \forall p.$$

Hence, \mathbf{A}^s is an M -matrix. This implies that $(\mathbf{A}^s)^{-1}$ is non-negative. Therefore, if $\vec{\mathbf{b}}^s \geq 0$, then it holds that $\vec{\rho}^{s+1} = (\mathbf{A}^s)^{-1} \vec{\mathbf{b}}^s \geq 0$.

Now, in order to get $\rho_{i,j}^{n+1,s+1} \geq 0$, it suffices to show $\vec{\mathbf{b}}^s \geq 0$, i.e., $b_{i,j}^s \geq 0$, $\forall i, j$. For convenience, we decompose $b_{i,j}^s \geq 0$ into the following two parts:

$$b_{i,j}^s = b_{i,j}^s(\vec{\mathbf{I}}^n) + b_{i,j}^s(\phi^n),$$

with

$$\begin{aligned}
b_{i,j}^s(\vec{\mathbf{I}}^n) &= \rho_{i,j}^n + \frac{\Delta t}{\Delta x} \left(\Phi_{i-1/2,j}^{n+1,s+1}(\vec{\mathbf{I}}^n) - \Phi_{i+1/2,j}^{n+1,s+1}(\vec{\mathbf{I}}^n) \right) + \\
&\quad \frac{\Delta t}{\Delta y} \left(\Upsilon_{i,j-1/2}^{n+1,s+1}(\vec{\mathbf{I}}^n) - \Upsilon_{i,j+1/2}^{n+1,s+1}(\vec{\mathbf{I}}^n) \right), \\
b_{i,j}^s(\phi^n) &= \frac{\Delta t}{\Delta x} \left(\Phi_{i-1/2,j}^{n+1,s+1}(\phi^n) - \Phi_{i+1/2,j}^{n+1,s+1}(\phi^n) \right) + \\
&\quad \frac{\Delta t}{\Delta y} \left(\Upsilon_{i,j-1/2}^{n+1,s+1}(\phi^n) - \Upsilon_{i,j+1/2}^{n+1,s+1}(\phi^n) \right) + \\
&\quad \frac{\sigma_{i,j}^{n+1,s} c \Delta t}{\epsilon^2} \kappa_{i,j}^{n+1,s} \phi_{i,j}^n.
\end{aligned}$$

Next, we show that $b_{i,j}^s(\vec{\mathbf{I}}^n) \geq 0$ and $b_{i,j}^s(\phi^n) \geq 0$.

First, denotes that

$$\begin{aligned}
\Phi_{i-1/2,j}^{n+1,s+1}(\vec{\mathbf{I}}^n) &= \tilde{\alpha}_{i-1/2,j}^{n+1,s} \left\{ \langle \xi \vec{\psi} \rangle_{1,4} \cdot \left(\vec{\mathbf{I}}_{i-1,j}^n + \frac{\Delta x}{2} \delta_x \vec{\mathbf{I}}_{i-1,j}^n \right) + \langle \xi \vec{\psi} \rangle_{2,3} \cdot \left(\vec{\mathbf{I}}_{i,j}^n - \frac{\Delta x}{2} \delta_x \vec{\mathbf{I}}_{i,j}^n \right) \right\} \\
&\quad + \tilde{b}_{i-1/2,j}^{n+1,s} \left(\langle \xi^2 \vec{\psi} \rangle_{1,4} \cdot \delta_x \vec{\mathbf{I}}_{i-1,j}^n + \langle \xi^2 \vec{\psi} \rangle_{2,3} \cdot \delta_x \vec{\mathbf{I}}_{i,j}^n \right).
\end{aligned}$$

And the expressions of $\Phi_{i+1/2,j}^{n+1,s+1}(\vec{\mathbf{I}}^n)$, $\Upsilon_{i,j-1/2}^{n+1,s+1}(\vec{\mathbf{I}}^n)$ and $\Upsilon_{i,j+1/2}^{n+1,s+1}(\vec{\mathbf{I}}^n)$ can be defined similarly. For $\Delta t > 0$, $\epsilon \geq 0$ and $\sigma \geq 0$, the coefficient function $\tilde{\alpha}(\Delta t, \epsilon, \sigma_{i,j}^{n+1,s}) \geq 0$. Applying (4.3) directly, one has

$$\begin{aligned}
\Phi_{i-1/2,j}^{n+1,s+1}(\vec{\mathbf{I}}^n) &\geq \tilde{\alpha}_{i-1/2,j}^{n+1,s} \langle \xi \vec{\psi} \rangle_{2,3} \cdot \left(\vec{\mathbf{I}}_{i,j}^n - \frac{\Delta x}{2} \delta_x \vec{\mathbf{I}}_{i,j}^n \right) \\
&\quad + \tilde{b}_{i-1/2,j}^{n+1,s} \langle \xi^2 \vec{\psi} \rangle_{2,3} \cdot \delta_x \vec{\mathbf{I}}_{i,j}^n, \\
-\Phi_{i+1/2,j}^{n+1,s+1}(\vec{\mathbf{I}}^n) &\geq -\tilde{\alpha}_{i+1/2,j}^{n+1,s} \langle \xi \vec{\psi} \rangle_{1,4} \cdot \left(\vec{\mathbf{I}}_{i,j}^n + \frac{\Delta x}{2} \delta_x \vec{\mathbf{I}}_{i,j}^n \right) \\
&\quad - \tilde{b}_{i+1/2,j}^{n+1,s} \langle \xi^2 \vec{\psi} \rangle_{1,4} \cdot \delta_x \vec{\mathbf{I}}_{i,j}^n.
\end{aligned}$$

Also by virtue of the conditions in (4.3), it holds that

$$\begin{aligned}
-\langle \xi \vec{\psi} \rangle_{2,3} \cdot \frac{\Delta x}{2} \delta_x \vec{\mathbf{I}}_{i,j}^n + \frac{\tilde{b}_{i-1/2,j}^{n+1,s}}{\tilde{\alpha}_{i-1/2,j}^{n+1,s}} \langle \xi^2 \vec{\psi} \rangle_{2,3} \cdot \delta_x \vec{\mathbf{I}}_{i,j}^n &\geq \langle \xi \vec{\psi} \rangle_{2,3} \cdot \vec{\mathbf{I}}_{i,j}^n, \\
-\langle \xi \vec{\psi} \rangle_{1,4} \cdot \frac{\Delta x}{2} \delta_x \vec{\mathbf{I}}_{i,j}^n - \frac{\tilde{b}_{i+1/2,j}^{n+1,s}}{\tilde{\alpha}_{i+1/2,j}^{n+1,s}} \langle \xi^2 \vec{\psi} \rangle_{1,4} \cdot \delta_x \vec{\mathbf{I}}_{i,j}^n &\geq -\langle \xi \vec{\psi} \rangle_{1,4} \cdot \vec{\mathbf{I}}_{i,j}^n.
\end{aligned}$$

Therefore,

$$\Phi_{i-1/2,j}^{n+1,s+1}(\vec{\mathbf{I}}^n) \geq 2\tilde{\alpha}_{i-1/2,j}^{n+1,s} \langle \xi \vec{\psi} \rangle_{2,3} \cdot \vec{\mathbf{I}}_{i,j}^n, \quad -\Phi_{i+1/2,j}^{n+1,s+1}(\vec{\mathbf{I}}^n) \geq -2\tilde{\alpha}_{i+1/2,j}^{n+1,s} \langle \xi \vec{\psi} \rangle_{1,4} \cdot \vec{\mathbf{I}}_{i,j}^n.$$

Similarly, by the conditions in (4.4), we can obtain

$$\Upsilon_{i,j-1/2}^{n+1,s+1}(\vec{\mathbf{I}}^n) \geq 2\tilde{\alpha}_{i,j-1/2}^{n+1,s} \langle \eta \vec{\psi} \rangle_{3,4} \cdot \vec{\mathbf{I}}_{i,j}^n, \quad -\Upsilon_{i,j+1/2}^{n+1,s+1}(\vec{\mathbf{I}}^n) \geq -2\tilde{\alpha}_{i,j+1/2}^{n+1,s} \langle \eta \vec{\psi} \rangle_{1,2} \cdot \vec{\mathbf{I}}_{i,j}^n.$$

Thus,

$$b_{i,j}^s(\vec{\mathbf{I}}^n) \geq \rho_{i,j}^n + \frac{\Delta t}{\Delta x} \left\{ 2\tilde{\alpha}_{i-1/2,j}^{n+1,s} \langle \xi \vec{\psi} \rangle_{2,3} \cdot \vec{\mathbf{I}}_{i,j}^n - 2\tilde{\alpha}_{i+1/2,j}^{n+1,s} \langle \xi \vec{\psi} \rangle_{1,4} \cdot \vec{\mathbf{I}}_{i,j}^n \right\} \\ + \frac{\Delta t}{\Delta y} \left\{ 2\tilde{\alpha}_{i,j-1/2}^{n+1,s} \langle \eta \vec{\psi} \rangle_{3,4} \cdot \vec{\mathbf{I}}_{i,j}^n - 2\tilde{\alpha}_{i,j+1/2}^{n+1,s} \langle \eta \vec{\psi} \rangle_{1,2} \cdot \vec{\mathbf{I}}_{i,j}^n \right\}.$$

Noticing that $\vec{\mathbf{I}}_{i,j}^n = (\frac{1}{2\sqrt{\pi}}\rho_{i,j}^n, \check{\vec{\mathbf{I}}}_{i,j}^n)'$, and

$$\langle \xi \psi_0^0 \rangle_{1,4} = \frac{\sqrt{\pi}}{2}, \quad \langle \xi \psi_0^0 \rangle_{2,3} = -\frac{\sqrt{\pi}}{2}, \quad \langle \eta \psi_0^0 \rangle_{1,2} = \frac{\sqrt{\pi}}{2}, \quad \langle \eta \psi_0^0 \rangle_{3,4} = -\frac{\sqrt{\pi}}{2},$$

we can rewrite $b_{i,j}^s(\vec{\mathbf{I}}^n)$ as

$$b_{i,j}^s(\vec{\mathbf{I}}^n) \geq \rho_{i,j}^n - \frac{\Delta t}{2} \left(\frac{\tilde{\alpha}_{i-1/2,j}^{n+1,s}}{\Delta x} + \frac{\tilde{\alpha}_{i+1/2,j}^{n+1,s}}{\Delta x} + \frac{\tilde{\alpha}_{i,j-1/2}^{n+1,s}}{\Delta y} + \frac{\tilde{\alpha}_{i,j+1/2}^{n+1,s}}{\Delta y} \right) \rho_{i,j}^n \\ + 2\Delta t \left\{ \frac{\tilde{\alpha}_{i-1/2,j}^{n+1,s}}{\Delta x} \langle \xi \check{\vec{\psi}} \rangle_{2,3} - \frac{\tilde{\alpha}_{i+1/2,j}^{n+1,s}}{\Delta x} \langle \xi \check{\vec{\psi}} \rangle_{1,4} + \frac{\tilde{\alpha}_{i,j-1/2}^{n+1,s}}{\Delta y} \langle \eta \check{\vec{\psi}} \rangle_{3,4} - \frac{\tilde{\alpha}_{i,j+1/2}^{n+1,s}}{\Delta y} \langle \eta \check{\vec{\psi}} \rangle_{1,2} \right\} \cdot \check{\vec{\mathbf{I}}}_{i,j}^n \\ \geq \rho_{i,j}^n - \Delta t \left(\frac{\tilde{\alpha}_{i-1/2,j}^{n+1,s}}{\Delta x} + \frac{\tilde{\alpha}_{i+1/2,j}^{n+1,s}}{\Delta x} + \frac{\tilde{\alpha}_{i,j-1/2}^{n+1,s}}{\Delta y} + \frac{\tilde{\alpha}_{i,j+1/2}^{n+1,s}}{\Delta y} \right) \rho_{i,j}^n \\ + \frac{\Delta t}{2} \left(\frac{\tilde{\alpha}_{i-1/2,j}^{n+1,s}}{\Delta x} + \frac{\tilde{\alpha}_{i+1/2,j}^{n+1,s}}{\Delta x} + \frac{\tilde{\alpha}_{i,j-1/2}^{n+1,s}}{\Delta y} + \frac{\tilde{\alpha}_{i,j+1/2}^{n+1,s}}{\Delta y} \right) \rho_{i,j}^n \\ + 2\Delta t \left\{ \frac{\tilde{\alpha}_{i-1/2,j}^{n+1,s}}{\Delta x} \langle \xi \check{\vec{\psi}} \rangle_{2,3} - \frac{\tilde{\alpha}_{i+1/2,j}^{n+1,s}}{\Delta x} \langle \xi \check{\vec{\psi}} \rangle_{1,4} + \frac{\tilde{\alpha}_{i,j-1/2}^{n+1,s}}{\Delta y} \langle \eta \check{\vec{\psi}} \rangle_{3,4} - \frac{\tilde{\alpha}_{i,j+1/2}^{n+1,s}}{\Delta y} \langle \eta \check{\vec{\psi}} \rangle_{1,2} \right\} \cdot \check{\vec{\mathbf{I}}}_{i,j}^n,$$

which together with (4.2) implies

$$b_{i,j}^s(\vec{\mathbf{I}}^n) \geq \rho_{i,j}^n - \Delta t \left(\frac{\tilde{\alpha}_{i-1/2,j}^{n+1,s}}{\Delta x} + \frac{\tilde{\alpha}_{i+1/2,j}^{n+1,s}}{\Delta x} + \frac{\tilde{\alpha}_{i,j-1/2}^{n+1,s}}{\Delta y} + \frac{\tilde{\alpha}_{i,j+1/2}^{n+1,s}}{\Delta y} \right) \rho_{i,j}^n.$$

Because for $\Delta t > 0, \epsilon \geq 0$ and $\sigma \geq 0$, the function $\tilde{\alpha}(\Delta t, \epsilon, \sigma)$ is decreasing with respect to the variable σ , we see that

$$0 < \tilde{\alpha}(\Delta t, \epsilon, \sigma_{i,j}^{n+1,s}) \leq \tilde{\alpha}(\Delta t, \epsilon, \min_{i,j} \sigma_{i,j}^{n+1,s}).$$

Thus,

$$b_{i,j}^s(\vec{\mathbf{I}}^n) \geq \left(1 - 2\Delta t \frac{\Delta x + \Delta y}{\Delta x \Delta y} \tilde{\alpha}(\Delta t, \epsilon, \min_{i,j} \sigma_{i,j}^{n+1,s}) \right) \rho_{i,j}^n.$$

Form the first constraint condition in (4.1) on time step Δt , we immediately get

$$b_{i,j}^s(\vec{\mathbf{I}}^n) \geq 0.$$

On the other hand,

$$\begin{aligned}
b_{i,j}^s(\phi^n) &= \frac{4\pi}{3} \frac{\Delta t}{\Delta x} \left(\tilde{d}_{i-1/2,j}^{n+1,s} \frac{\kappa_{i,j}^{n+1,s} \phi_{i,j}^n - \kappa_{i-1,j}^{n+1,s} \phi_{i-1,j}^n}{\Delta x} - \tilde{d}_{i+1/2,j}^{n+1,s} \frac{\kappa_{i+1,j}^{n+1,s} \phi_{i+1,j}^n - \kappa_{i,j}^{n+1,s} \phi_{i,j}^n}{\Delta x} \right) \\
&+ \frac{4\pi}{3} \frac{\Delta t}{\Delta y} \left(\tilde{d}_{i,j-1/2}^{n+1,s} \frac{\kappa_{i,j}^{n+1,s} \phi_{i,j}^n - \kappa_{i,j-1}^{n+1,s} \phi_{i,j-1}^n}{\Delta y} - \tilde{d}_{i,j+1/2}^{n+1,s} \frac{\kappa_{i,j+1}^{n+1,s} \phi_{i,j+1}^n - \kappa_{i,j}^{n+1,s} \phi_{i,j}^n}{\Delta y} \right) \\
&+ \frac{\sigma_{i,j}^{n+1,s} c \Delta t}{\epsilon^2} \kappa_{i,j}^{n+1,s} \phi_{i,j}^n = \Delta t \kappa_{i,j}^{n+1,s} \\
&\left(\frac{\sigma_{i,j}^{n+1,s} c}{\epsilon^2} + \frac{4\pi}{3(\Delta x)^2} (\tilde{d}_{i-1/2,j}^{n+1,s} + \tilde{d}_{i+1/2,j}^{n+1,s}) + \frac{4\pi}{3(\Delta y)^2} (\tilde{d}_{i,j-1/2}^{n+1,s} + \tilde{d}_{i,j+1/2}^{n+1,s}) \right) \phi_{i,j}^n \\
&- \frac{4\pi}{3} \frac{\Delta t}{(\Delta x)^2} \tilde{d}_{i-1/2,j}^{n+1,s} \kappa_{i-1,j}^{n+1,s} \phi_{i-1,j}^n - \frac{4\pi}{3} \frac{\Delta t}{(\Delta x)^2} \tilde{d}_{i+1/2,j}^{n+1,s} \kappa_{i+1,j}^{n+1,s} \phi_{i+1,j}^n \\
&- \frac{4\pi}{3} \frac{\Delta t}{(\Delta y)^2} \tilde{d}_{i,j-1/2}^{n+1,s} \kappa_{i,j-1}^{n+1,s} \phi_{i,j-1}^n - \frac{4\pi}{3} \frac{\Delta t}{(\Delta y)^2} \tilde{d}_{i,j+1/2}^{n+1,s} \kappa_{i,j+1}^{n+1,s} \phi_{i,j+1}^n.
\end{aligned}$$

For $\tilde{d}(\Delta t, \epsilon, \sigma) \leq 0$ and $\kappa = \frac{\epsilon^2}{\epsilon^2 + \Delta t \beta \sigma} \geq 0$, one has

$$\begin{aligned}
&b_{i,j}^s(\phi^n) \\
&\geq \Delta t \kappa_{i,j}^{n+1,s} \left(\frac{\sigma_{i,j}^{n+1,s} c}{\epsilon^2} + \frac{4\pi}{3(\Delta x)^2} (\tilde{d}_{i-1/2,j}^{n+1,s} + \tilde{d}_{i+1/2,j}^{n+1,s}) + \frac{4\pi}{3(\Delta y)^2} (\tilde{d}_{i,j-1/2}^{n+1,s} + \tilde{d}_{i,j+1/2}^{n+1,s}) \right) \phi_{i,j}^n \\
&\geq \Delta t \kappa_{i,j}^{n+1,s} \sigma_{i,j}^{n+1,s} \left(\frac{c}{\epsilon^2} + \frac{4\pi}{3} \left(\frac{2}{(\Delta x)^2} + \frac{2}{(\Delta y)^2} \right) \frac{\min\{\tilde{d}_{i,j\pm 1/2}^{n+1,s}, \tilde{d}_{i\pm 1/2,j}^{n+1,s}\}}{\sigma_{i,j}^{n+1,s}} \right) \phi_{i,j}^n.
\end{aligned}$$

From the second time step constraint condition in (4.1), one obtains

$$b_{i,j}^s(\phi^n) \geq 0.$$

This completes the proof. \square

Remark 4.1. We remark that the conditions (4.1) on Δt are not restrictive. (i) For the optically thin case ($\epsilon = O(1), \sigma \rightarrow 0$), since $\tilde{\alpha} \rightarrow \frac{\epsilon}{c}$, the first time step constraint condition in (4.1) can be simplified to $\Delta t \leq \frac{\epsilon}{4c} \cdot \min\{\Delta x, \Delta y\}$. And by the analysis used in [40, Appendix], the second time step constraint condition in (4.1) can be reduced to $\Delta t \leq \frac{\sqrt{6}}{2} \cdot \frac{\epsilon}{c} \cdot \min\{\Delta x, \Delta y\}$. Thus, for the optically thin case ($\epsilon = O(1), \sigma \rightarrow 0$), the time step constraint conditions in (4.1) reduce to

$$\Delta t \leq \frac{\epsilon}{4c} \cdot \min\{\Delta x, \Delta y\}, \quad (4.5)$$

which happens to be the usual CFL stability condition $\Delta t \leq CFL \cdot \frac{\epsilon}{c} \min\{\Delta x, \Delta y\}$ with $CFL = \frac{1}{4}$. (ii) For the optically thick case ($\epsilon \rightarrow 0, \sigma = O(1)$), since $\tilde{\alpha} \rightarrow 0$ and $\tilde{d} \rightarrow -c/(4\pi\sigma)$, we see that there is actually no constraint on the time step.

4.2 Realizability of limiters

In this subsection, we show that with suitable scaling limiters the conditions (4.2)-(4.4) in Theorem 4.1 can be realized. First, it is easy to see that if the reconstructed initial data in the x - and y -directions are nonnegative, i.e.,

$$\vec{\psi} \cdot (\vec{\mathbf{I}}_{i,j}^n + \delta_x \vec{\mathbf{I}}_{i,j}^n(x - x_i)) \geq 0, \quad \forall x \in (x_{i-1/2}, x_{i+1/2}), \quad (4.6)$$

$$\vec{\psi} \cdot (\vec{\mathbf{I}}_{i,j}^n + \delta_y \vec{\mathbf{I}}_{i,j}^n(y - y_j)) \geq 0, \quad \forall y \in (y_{j-1/2}, y_{j+1/2}), \quad (4.7)$$

we can verify that the conditions (4.2)-(4.4) hold under a reasonable time step.

In fact, with the nonnegative reconstructions (4.6) and (4.7), by setting $x = x_i, y = y_j$, we first find the nonnegative P_N -reconstruction for the angular variable, i.e., $\vec{\psi} \cdot \vec{\mathbf{I}}_{i,j}^n \geq 0$. This immediately implies $\langle (1 \pm \xi) \vec{\psi} \cdot \vec{\mathbf{I}}^n \rangle_{1,4 \text{ or } 2,3} \geq 0$ and $\langle (1 \pm \eta) \vec{\psi} \cdot \vec{\mathbf{I}}^n \rangle_{1,2 \text{ or } 3,4} \geq 0$. Based on these results, it is easy to verify that the condition (4.2) holds for the case $\tilde{\alpha}_{i\pm 1/2,j}^{n+1,s} = \tilde{\alpha}_{i,j\pm 1/2}^{n+1,s}$. Then, if we follow the nonnegative piecewise linear reconstruction for the spatial variable in (3.11)-(3.13) and assume that Δt satisfies

$$\max_{i'=i\pm 1/2, j'=j\pm 1/2} \frac{-\tilde{b}_{i',j'}^{n+1,s}(\Delta t)}{\tilde{\alpha}_{i',j'}^{n+1,s}(\Delta t)} \leq \min\{\Delta x, \Delta y\}, \quad (4.8)$$

thus for

$$x = \begin{cases} x_{i\pm 1/2} \pm \frac{\tilde{b}_{i\pm 1/2,j}^{n+1,s}}{\tilde{\alpha}_{i\pm 1/2,j}^{n+1,s}} \xi, & \text{if } \xi \geq 0, \\ x_{i\pm 1/2} \mp \frac{\tilde{b}_{i\pm 1/2,j}^{n+1,s}}{\tilde{\alpha}_{i\pm 1/2,j}^{n+1,s}} \xi, & \text{if } \xi < 0, \end{cases} \quad y = \begin{cases} y_{i\pm 1/2} \pm \frac{\tilde{b}_{i,j\pm 1/2}^{n+1,s}}{\tilde{\alpha}_{i,j\pm 1/2}^{n+1,s}} \eta, & \text{if } \eta \geq 0, \\ y_{i\pm 1/2} \mp \frac{\tilde{b}_{i,j\pm 1/2}^{n+1,s}}{\tilde{\alpha}_{i,j\pm 1/2}^{n+1,s}} \eta, & \text{if } \eta < 0, \end{cases}$$

we have $x \in (x_{i-1/2}, x_{i+1/2}), y \in (y_{j-1/2}, y_{j+1/2})$.

Substituting the above x, y into (4.6)-(4.7) and multiplying ξ, η respectively in (4.6)-(4.7), we integrate with respect to the angular variable to verify that the conditions in (4.3)-(4.4) hold. This implies that, under the time step constraint (4.8), the conditions (4.2)-(4.4) hold automatically if the piecewise linear reconstruction of the initial intensities are nonnegative. We remark here that although the added time step constraint (4.8) is needed, it will be clarified in Remark 4.2 that (4.8) is in fact not restrictive.

Generally, the reconstruction of the initial intensity could be negative. In order to make the conditions (4.2)-(4.4) valid in this case, the scaling limiters will be used in this paper. Notice that the condition (4.2) also appears in the positive-preserving needing conditions of our previous constructed first-order scheme [39]. Therefore, as done there, we tune the micro coefficients $\check{\mathbf{I}}_{i,j}^n$ uniformly, while keeping the macro quantity $\rho_{i,j}^n$ unchanged, so as to make the condition (4.2) as well as the following conditions hold:

$$\begin{aligned} \frac{1}{4} \rho_{i,j}^n + \langle \xi \check{\vec{\psi}} \rangle_{1,4} \cdot \check{\mathbf{I}}_{i,j}^n &\geq 0, & \frac{1}{4} \rho_{i,j}^n - \langle \xi \check{\vec{\psi}} \rangle_{2,3} \cdot \check{\mathbf{I}}_{i,j}^n &\geq 0, \\ \frac{1}{4} \rho_{i,j}^n + \langle \eta \check{\vec{\psi}} \rangle_{1,2} \cdot \check{\mathbf{I}}_{i,j}^n &\geq 0, & \frac{1}{4} \rho_{i,j}^n - \langle \eta \check{\vec{\psi}} \rangle_{3,4} \cdot \check{\mathbf{I}}_{i,j}^n &\geq 0. \end{aligned} \quad (4.9)$$

This can be achieved by using the linear scaling (ls) limiter from [42]. That is, one replaces $\check{\vec{\mathbf{I}}}_{i,j}^n$ by $\lambda_{i,j}^1 \check{\vec{\mathbf{I}}}_{i,j}^n$, with $\lambda_{i,j}^1$ given by

$$\lambda_{i,j}^1 = \operatorname{argmax}_{\lambda \in [0,1]} \{ \lambda : \lambda \check{\vec{\mathbf{I}}}_{i,j}^n \text{ satisfies conditions in (4.2) and (4.9)} \}. \quad (4.10)$$

Since $\rho_{i,j}^n \geq 0$, the positive limiter in (4.10) is realizable. With this modified P_N -reconstruction (here we slightly abuse the notation and still denote it by $\vec{\psi} \cdot \vec{\mathbf{I}}_{i,j}^n$), we modify the reconstruction slopes $\delta_x \vec{\mathbf{I}}_{i,j}^n$ and $\delta_y \vec{\mathbf{I}}_{i,j}^n$ to make (4.3) and (4.4) hold, respectively. For simplicity, the modifications are employed uniformly, i.e., one need replace $\delta_x \vec{\mathbf{I}}_{i,j}^n$ and $\delta_y \vec{\mathbf{I}}_{i,j}^n$ by $\lambda_{i,j}^{21} \delta_x \vec{\mathbf{I}}_{i,j}^n$ and $\lambda_{i,j}^{22} \delta_y \vec{\mathbf{I}}_{i,j}^n$ respectively, with $\lambda_{i,j}^{21}, \lambda_{i,j}^{22}$ given by

$$\lambda_{i,j}^{21} = \operatorname{argmax}_{\lambda \in [0,1]} \{ \lambda : \lambda \delta_x \vec{\mathbf{I}}_{i,j}^n, \text{ satisfies conditions in (4.3)} \}, \quad (4.11)$$

$$\lambda_{i,j}^{22} = \operatorname{argmax}_{\lambda \in [0,1]} \{ \lambda : \lambda \delta_y \vec{\mathbf{I}}_{i,j}^n \text{ satisfies conditions in (4.4)} \}. \quad (4.12)$$

Noticing that the modified P_N -reconstruction $\vec{\psi} \cdot \vec{\mathbf{I}}_{i,j}^n$ satisfies the inequalities in (4.9), which can be rewritten as

$$\langle \xi \vec{\psi} \rangle_{1,4} \cdot \vec{\mathbf{I}}_{i,j}^n \geq 0, \quad \langle -\xi \vec{\psi} \rangle_{2,3} \cdot \vec{\mathbf{I}}_{i,j}^n \geq 0, \quad \langle \eta \vec{\psi} \rangle_{1,2} \cdot \vec{\mathbf{I}}_{i,j}^n \geq 0, \quad \langle -\eta \vec{\psi} \rangle_{3,4} \cdot \vec{\mathbf{I}}_{i,j}^n \geq 0.$$

Thus, the limiters in (4.11) and (4.12) are realizable, and the conditions in (4.3)-(4.4) are hence satisfied.

We remark that using the positive P_N closures in [14] or the positive filtered P_N closures in [22] can also yield the desired positive scheme. It is, however, computationally expensive. So, following the construction procedure in [21] and of our previous first-order scheme [39], here we apply much cheap linear scaling limiters to achieve the positive property.

By incorporating the above positive-preserving (PP) limiters into the FP_N -based UGKS, we obtain the so-called $PPFP_N$ -based UGKS by following almost the same procedure as in the "Loop of the FP_N -based UGKS" in Subsection 3.3 except that, before solving the linearized macro equations (3.19)-(3.20) and the micro equations (3.5), the micro coefficients $\check{\vec{\mathbf{I}}}_{i,j}^n$ in the fluxes have to be replaced by $\lambda_{i,j}^1 \check{\vec{\mathbf{I}}}_{i,j}^n$ for each spatial cell (i, j) first, and then replace $\delta_x \vec{\mathbf{I}}_{i,j}^n, \delta_y \vec{\mathbf{I}}_{i,j}^n$ by $\lambda_{i,j}^{21} \delta_x \vec{\mathbf{I}}_{i,j}^n, \lambda_{i,j}^{22} \delta_y \vec{\mathbf{I}}_{i,j}^n$.

Remark 4.2. For the optically thin case ($\epsilon = O(1), \sigma \rightarrow 1$), the condition (4.8) reduces to $\Delta t \leq \frac{2\epsilon}{c} \min\{\Delta x, \Delta y\}$, which is induced by the fact that $\frac{\tilde{b}}{\alpha} \rightarrow -\frac{c\Delta t}{2\epsilon}$. Thus, in combination with (4.5), the final positive preserving time step constraint takes the following form:

$$\Delta t \leq \frac{\epsilon}{4c} \cdot \min\{\Delta x, \Delta y\}. \quad (4.13)$$

On the other hand, for the optically thick case ($\epsilon \rightarrow 1, \sigma = O(1)$), as $\frac{\tilde{b}}{\alpha}$ tends to zero, we see that the condition (4.8) actually does not impose any constraints on the time step.

4.3 Asymptotic analysis

In this subsection we analyze the asymptotic preserving (AP) property of the above developed $PPFP_N$ -based UGKS scheme. In fact, the asymptotic behavior of the algorithm in the small ϵ limit is completely determined by the coefficient functions, which are given by

Proposition 4.1. *Let σ be positive and $\Delta t = O(1)$. Then as $\epsilon \rightarrow 0$, we have*

- $\tilde{\alpha}(\Delta t, \epsilon, \sigma, \nu)$ and $\tilde{b}(\Delta t, \epsilon, \sigma, \nu)$ tend to 0;
- $\frac{\epsilon}{c}\tilde{c}(\Delta t, \epsilon, \sigma, \nu)$ tends to $\frac{1}{4\pi}$;
- $\tilde{d}(\Delta t, \epsilon, \sigma, \nu)$ tends to $-\frac{c}{4\pi\sigma}$.

With Proposition 4.1 in hand, we can show the desired asymptotic preserving property of the proposed numerical scheme in the following theorem.

Theorem 4.2. *Let σ be positive, and $(\Delta x, \Delta y, \Delta t) = O(1)$. Then, as ϵ tends to zero, the $PPFP_N$ -based UGKS scheme for the equations (2.3) approaches to a standard positive-preserving implicit diffusion scheme for the diffusion limit equation (2.2).*

Proof. By Remark 4.2, we know that as $\epsilon \rightarrow 0$, there is no constraint on the time step. And also from Proposition 4.1, one has $\tilde{\alpha}, \tilde{b} \xrightarrow{\epsilon \rightarrow 0} 0$. Therefore, the positive-preserving limiters do not act on the solution at all for this optically thick limit case. In other words, they can be omitted in this case. Thus, we only need to focus on analyzing the discrete macro and micro equations (3.4)–(3.5).

Recalling that $\kappa = \frac{\epsilon^2}{\epsilon^2 + \Delta t \beta \sigma} \xrightarrow{\epsilon \rightarrow 0} 0$, and following almost the same process as in the proof of Theorem 4.1 in [39], we can obtain the asymptotic preserving property of the proposed $PPFP_N$ -based UGKS scheme as $\epsilon \rightarrow 0$. This completes the proof. \square

5 Simplified $PPFP_N$ -based UGKS

The numerical fluxes in the above $PPFP_N$ -based UGKS are of spatial second-order accuracy for (2.3). Compared with the fluxes of the first-order scheme in [39], the flux expressions in (3.14)–(3.15) and (3.17)–(3.18) are quite complex. In this section we shall show that in the regime $\epsilon \ll 1$ and the regime $\epsilon = O(1)$, the fluxes can be simplified, while the positive preserving and asymptotic preserving properties can be still kept. Thus, a simplified $PPFP_N$ -based UGKS (abbreviated as the $PPFP_N$ -based SUGKS) is obtained and the computational costs can be reduced greatly.

In order to simplify the fluxes in (3.14)–(3.15), we denote

$$\begin{aligned} \Phi_{i-1/2,j}^{n+1}(\tilde{b}) &= \tilde{b}_{i-1/2,j}^{n+1} \left(\langle \xi^2 \vec{\psi} \rangle_{1,4} \cdot \delta_x \vec{I}_{i-1,j}^n + \langle \xi^2 \vec{\psi} \rangle_{2,3} \cdot \delta_x \vec{I}_{i,j}^n \right), \\ G_{i-1/2,j}(\tilde{b}) &= \tilde{b}_{i-1/2,j}^{n+1} \left(\langle \xi^2 \psi_\ell^m \vec{\psi} \rangle_{1,4} \cdot \delta_x \vec{I}_{i-1,j}^n + \langle \xi^2 \psi_\ell^m \vec{\psi} \rangle_{2,3} \cdot \delta_x \vec{I}_{i,j}^n \right), \end{aligned}$$

$$G_{i-1/2,j}(\tilde{c}) = \tilde{c}_{i-1/2,j}^{n+1} \langle \xi \psi_\ell^m \rangle \left((\kappa^{n+1} \phi^n)_{i-1/2,j} + (1 - \kappa_{i-1/2,j}^{n+1}) \rho_{i-1/2,j}^{n+1} \right),$$

where function G denotes the components of the vector $\vec{\mathbf{G}}$ for $1 \leq \ell \leq N, -\ell \leq m \leq \ell$. We point out that the other fluxes can be handled in a similar way. In the following, we use " \lesssim " to denote " $\leq C$ " with C being a nonnegative constant independent of $\epsilon, \Delta x, \Delta y$ and Δt . By a detailed derivation that is given in Appendix 8, we obtain the following lemma:

Lemma 5.1. *Assume that σ, C_ν and the solution of (2.3) are sufficiently smooth. Then, it holds that*

$$\left| \frac{\Phi_{i-1/2,j}^{n+1}(\tilde{b}) - \Phi_{i+1/2,j}^{n+1}(\tilde{b})}{\Delta x} + \frac{\Upsilon_{i,j-1/2}^{n+1}(\tilde{b}) - \Upsilon_{i,j+1/2}^{n+1}(\tilde{b})}{\Delta y} \right| \lesssim \Delta t, \quad (5.1)$$

$$\left| \frac{G_{i-1/2,j}(\tilde{b}) - G_{i+1/2,j}(\tilde{b})}{\Delta x} + \frac{H_{i,j-1/2}(\tilde{b}) - H_{i,j+1/2}(\tilde{b})}{\Delta y} \right| \lesssim \Delta t, \quad (5.2)$$

in the regimes $\epsilon \ll 1$ and $\epsilon = O(1)$. And

$$\epsilon^2 \left| \frac{G_{i-1/2,j}(\tilde{c}) - G_{i+1/2,j}(\tilde{c})}{\Delta x} + \frac{H_{i,j-1/2}(\tilde{c}) - H_{i,j+1/2}(\tilde{c})}{\Delta y} \right| \lesssim \Delta t \text{ in the regime } \epsilon \ll 1, \quad (5.3)$$

$$\left| \frac{G_{i-1/2,j}(\tilde{c}) - G_{i+1/2,j}(\tilde{c})}{\Delta x} + \frac{H_{i,j-1/2}(\tilde{c}) - H_{i,j+1/2}(\tilde{c})}{\Delta y} \right| \lesssim \Delta t \text{ in the regime } \epsilon = O(1). \quad (5.4)$$

Now with the help of Lemma 5.1, in the regimes $\epsilon \ll 1$ and $\epsilon = O(1)$, one can estimate the contribution of each term on the left hand sides of (5.1)-(5.4) to the final solution. For this, we shall analyze the contribution to the macro solution and micro solution respectively. Firstly, by the linearized macro equations (3.19), we use the notion

$$\Delta \vec{\rho}^{s+1} = (\Delta \rho_{1,1}^{n+1,s+1}, \Delta \rho_{1,2}^{n+1,s+1}, \dots, \Delta \rho_{2,1}^{n+1,s+1}, \Delta \rho_{2,2}^{n+1,s+1}, \dots)'$$

to represent the solution of the following equation in matrix form:

$$\mathbf{A}^s \Delta \vec{\rho}^{s+1} = \vec{z}^s,$$

where \mathbf{A}^s is the coefficient matrix of (3.19), and $\vec{z}^s = (z_{1,1}^{n+1,s}, z_{1,2}^{n+1,s}, \dots, z_{2,1}^{n+1,s}, z_{2,2}^{n+1,s}, \dots)'$ with

$$z_{i,j}^{n+1,s} = \Delta t \left(\frac{\Phi_{i-1/2,j}^{n+1,s+1}(\tilde{b}) - \Phi_{i+1/2,j}^{n+1,s+1}(\tilde{b})}{\Delta x} + \frac{\Upsilon_{i,j-1/2}^{n+1,s+1}(\tilde{b}) - \Upsilon_{i,j+1/2}^{n+1,s+1}(\tilde{b})}{\Delta y} \right).$$

Namely, $\Delta \rho_{i,j}^{n+1,s+1}$ shows the contribution of the term in (5.1) to the macro solution $\rho_{i,j}^{n+1}$. Since the coefficient matrix \mathbf{A}^s can be decomposed into $\mathbf{A}^s = \mathbf{E} - \mathbf{B}^s$ with \mathbf{E} being the identity matrix, and \mathbf{B}^s satisfying $\mathbf{B}^s(i, j) \geq 0 (i \neq j)$ and $\sum_j \mathbf{B}^s(i, j) \leq 0$ for all i , we see that $\|(\mathbf{A}^s)^{-1}\|_\infty \leq 1$. Consequently,

$$\|\Delta \vec{\rho}^{s+1}\|_\infty = \|(\mathbf{A}^s)^{-1} \vec{z}^s\|_\infty \leq \|(\mathbf{A}^s)^{-1}\|_\infty \|\vec{z}^s\|_\infty \leq \|\vec{z}^s\|_\infty.$$

From (5.1) one gets $\|\tilde{\mathbf{z}}^s\|_\infty \lesssim (\Delta t)^2$. Therefore, $|\Delta \rho_{i,j}^{n+1,s+1}| \lesssim (\Delta t)^2$ follows immediately. In addition, from (3.20), the contribution to the macro solution $\phi_{i,j}^{n+1}$ reads as

$$\Delta \phi_{i,j}^{n+1,s+1} \equiv (1 - \kappa_{i,j}^{n+1,s}) \Delta \rho_{i,j}^{n+1,s+1}.$$

Since $\kappa = \frac{\epsilon^2}{\epsilon^2 + \Delta t \beta \sigma} \in [0, 1]$, thus $|\Delta \phi_{i,j}^{n+1,s+1}| \lesssim (\Delta t)^2$ holds.

Secondly, in view of (3.5), that

$$\begin{aligned} \check{\mathbf{I}}_{i,j}^{n+1} &= \left(\left(1 + \frac{\sigma_{i,j}^{n+1} c \Delta t}{\epsilon^2} \right) \mathbf{E} + \Delta t \sigma_f \check{\mathbf{F}} \right)^{-1} \times \\ &\quad \left\{ \check{\mathbf{I}}_{i,j}^n + \Delta t \left(\frac{\vec{\mathbf{G}}_{i-1/2,j} - \vec{\mathbf{G}}_{i+1/2,j}}{\Delta x} + \frac{\vec{\mathbf{H}}_{i,j-1/2} - \vec{\mathbf{H}}_{i,j+1/2}}{\Delta y} \right) \right\}. \end{aligned} \quad (5.5)$$

Recalling that $\check{\mathbf{F}}$ is a diagonal matrix, from (5.5), the contribution of the term in (5.2) to the micro solution $(I_\ell^m)_{i,j}^{n+1}$ takes the following form

$$\begin{aligned} \Delta_{\tilde{b}}(I_\ell^m)_{i,j}^{n+1} &\equiv \frac{\Delta t}{1 + \frac{\sigma_{i,j}^{n+1} c \Delta t}{\epsilon^2} + \Delta t \sigma_f \mathbf{F}_{(\ell,m),(\ell,m)}} \times \\ &\quad \left(\frac{G_{i-1/2,j}(\tilde{b}) - G_{i+1/2,j}(\tilde{b})}{\Delta x} + \frac{H_{i,j-1/2}(\tilde{b}) - H_{i,j+1/2}(\tilde{b})}{\Delta y} \right). \end{aligned}$$

In view of (5.2) and the fact that $\mathbf{F}_{(\ell,m),(\ell,m)}$ is nonnegative, we immediately get

$$|\Delta_{\tilde{b}}(I_\ell^m)_{i,j}^{n+1}| \lesssim (\Delta t)^2.$$

Futhermore, for

$$\begin{aligned} \Delta_{\tilde{c}}(I_\ell^m)_{i,j}^{n+1} &\equiv \frac{\Delta t}{1 + \frac{\sigma_{i,j}^{n+1} c \Delta t}{\epsilon^2} + \Delta t \sigma_f \mathbf{F}_{(\ell,m),(\ell,m)}} \times \\ &\quad \left(\frac{G_{i-1/2,j}(\tilde{c}) - G_{i+1/2,j}(\tilde{c})}{\Delta x} + \frac{H_{i,j-1/2}(\tilde{c}) - H_{i,j+1/2}(\tilde{c})}{\Delta y} \right). \end{aligned}$$

Similarly we can obtain $|\Delta_{\tilde{c}}(I_\ell^m)_{i,j}^{n+1}| \lesssim (\Delta t)^2$. Thus, we summarize the results in the following theorem:

Theorem 5.1. *Assume that σ, C_ν and the solution of (2.3) are sufficiently smooth. Then, in the regime $\epsilon \ll 1$ and the regime $\epsilon = O(1)$, it holds that*

$$|\Delta \phi_{i,j}^{n+1,s+1}| \lesssim (\Delta t)^2, \quad |\Delta \rho_{i,j}^{n+1,s+1}| \lesssim (\Delta t)^2, \quad (5.6)$$

and

$$|\Delta_{\tilde{b}}(I_\ell^m)_{i,j}^{n+1}| \lesssim (\Delta t)^2, \quad |\Delta_{\tilde{c}}(I_\ell^m)_{i,j}^{n+1}| \lesssim (\Delta t)^2. \quad (5.7)$$

Because the first-order discretization for the temporal variable is used in the scheme of the above section, and Theorem 5.1 implies that, in the regime $\epsilon \ll 1$ and the regime

$\epsilon = O(1)$, the contribution of the corresponding terms in Theorem 5.1 to the final solutions are the high-order terms with respect to Δt , we can delete these terms from the fluxes directly to simplify the fluxes but without reducing the accuracy in the temporal variable. We call this simplification the simplified $PPFP_N$ -based UGKS. As a result, in the regime $\epsilon \ll 1$ and the regime $\epsilon = O(1)$, for the x -direction as example, the simplified macro and micro fluxes read as

$$\begin{aligned}\mathring{\Phi}_{i-1/2,j}^{n+1} &= \tilde{\alpha}_{i-1/2,j}^{n+1} \left\{ \langle \xi \vec{\psi} \rangle_{1,4} \cdot \left(\vec{I}_{i-1,j}^n + \frac{\Delta x}{2} \delta_x \vec{I}_{i-1,j}^n \right) + \langle \xi \vec{\psi} \rangle_{2,3} \cdot \left(\vec{I}_{i,j}^n - \frac{\Delta x}{2} \delta_x \vec{I}_{i,j}^n \right) \right\} \\ &\quad + \tilde{d}_{i-1/2,j}^{n+1} \frac{4\pi}{3} \left(\delta_x (\kappa^{n+1} \phi^n)_{i-1/2,j} + (1 - \kappa_{i-1/2,j}^{n+1}) \delta_x \rho_{i-1/2,j}^{n+1} \right), \\ \mathring{\mathbf{G}}_{i-1/2,j} &= \tilde{\alpha}_{i-1/2,j}^{n+1} \left\{ \langle \xi \check{\psi} \check{\psi}' \rangle_{1,4} \cdot \left(\vec{I}_{i-1,j}^n + \frac{\Delta x}{2} \delta_x \vec{I}_{i-1,j}^n \right) + \langle \xi \check{\psi} \check{\psi}' \rangle_{2,3} \cdot \left(\vec{I}_{i,j}^n - \frac{\Delta x}{2} \delta_x \vec{I}_{i,j}^n \right) \right\} \\ &\quad + \tilde{d}_{i-1/2,j}^{n+1} \langle \xi^2 \check{\psi} \rangle \left(\delta_x (\kappa^{n+1} \phi^n)_{i-1/2,j} + (1 - \kappa_{i-1/2,j}^{n+1}) \delta_x \rho_{i-1/2,j}^{n+1} \right).\end{aligned}$$

Similar expressions can be taken for $\mathring{\Upsilon}_{i,j-1/2}^{n+1}$, $\mathring{\mathbf{H}}_{i,j-1/2}$ in the y -direction.

In view of the simplified fluxes, it is easy to find that they are in fact a direct combination of the simplest second-order upwind fluxes for the optically thin regime and the second-order fluxes for the diffusion limit. And UGKS just provides the combination coefficients, i.e, multi-scale coefficients that make the scheme possess the multi-scale property. We also remind that these fluxes can not be simplified any more in the intermediate regime. And in this case, it is better to keep all the terms in the fluxes (3.14)-(3.15) and (3.17)-(3.18), i.e., the original $PPFP_N$ -based UGKS is preferred.

In the regime $\epsilon \ll 1$ and the regime $\epsilon = O(1)$, replacing all the fluxes in the $PPFP_N$ -based UGKS scheme with the above simplified fluxes, which have no effect on the positive preserving and asymptotic preserving properties, will result in the desired simplified $PPFP_N$ -based UGKS, i.e., the $PPFP_N$ -based SUGKS.

6 Numerical experiments

In this section we test the performance of the proposed second order AP and PP schemes, i.e., the $PPFP_N$ -based UGKS and $PPFP_N$ -based SUGKS, which we abbreviate as $PPFP_N$ and $PPFP_N$ -S in the following.

As for the time step Δt , it is taken to satisfy the positive-preserving constraint conditions (4.1), (4.8) and the CFL stability condition. Here the CFL condition is determined by using an argument similar to that used in [27], and as a result, the following CFL condition will be used in our numerical experiments:

$$\Delta t \leq CFL \cdot \min\{\Delta x, \Delta y\},$$

where $CFL < 1$ is some problem-dependent constant.

First in Examples 1 and 2, we consider the following linear radiation transfer equation, which is a simplification of the system (2.1) in the case that the material temperature and the radiation temperature are the same

$$\frac{\epsilon^2}{c} \partial_t I + \epsilon \boldsymbol{\Omega} \cdot \nabla I = \sigma \left(\frac{1}{4\pi} \rho - I \right). \quad (6.1)$$

EXAMPLE 1 (The line source problem). This problem serves as a benchmark test in studying various angular approaches [9] in dealing with the ray effects. We present the problem specifications in Table 1. The numerical simulation is run on 150×150 spatial meshes with time step $\Delta t = 0.1 \cdot \min\{\Delta x, \Delta y\}$, which satisfies the positive preserving constraint conditions and the CFL condition. The final simulation time is $t = 1$. The spherical-spline filter function $f_{\text{SSpline}}(\lambda) = \frac{1}{1+\lambda^4}$ and $\sigma_f = 45$ are applied. Figures 1 and 2 show the contours of the solution ρ and the line-outs along the nonnegative x -axis and $y = x$ at time $t = 1$. Moreover, the exact solution in [10], as well as the S_{16} and P_{11} solutions, and in particular, the solution of the first-order $PPFP_{11}$ scheme (abbreviate as $PPFP_{11}^{1\text{-order}}$ in the following) constructed in our previous work [39] with 300×300 spatial meshes are also plotted in Figures 1 and 2 for comparison.

Table 1: Problem specifications of EXAMPLE 1.

| | |
|----------------------|--|
| Spatial domain: | $[-1.5, 1.5] \times [-1.5, 1.5]$ |
| Parameters: | $\sigma = 1, c = 1, \epsilon = 1$ |
| Boundary conditions: | all are vacuum |
| Initial condition: | $I(x, y, \boldsymbol{\Omega}, 0) \approx \frac{1}{4\pi} \left(\frac{1}{2\pi\zeta^2} e^{-\frac{x^2+y^2}{2\zeta^2}} \right)$ with $\zeta = 0.03$ |

It can be seen from Figures 1-2 that the S_{16} solution and P_{11} solution perform poorly due to ray effects and oscillations, respectively. Furthermore, negative ρ can be clearly observed in the P_{11} approximation. On the other hand, the first-order $PPFP_{11}$ solution, the current second-order $PPFP_{11}$ solution and $PPFP_{11}\text{-}S$ solution not only have higher accuracy, but also can suppress the oscillations of the P_{11} solution and maintain the positivity of the solution.

In Table 2, we give the relative ℓ_2 spatial errors of ρ at $t = 1$ (denoted by $re(\ell_2^{\rho})$) and the computation time of these schemes. The numerical tests are carried out on a Lenovo personal computer with Intel(R) Core(TM) i7-8700 CPU. It can be seen from Table 2 that the current second-order schemes indeed perform better in accuracy than S_{16} and P_{11} . Furthermore, the current schemes are computationally efficient as well. In particular, by comparing the $PPFP_{11}^{1\text{-order}}$ scheme with the $PPFP_{11}\text{-}S$ scheme, we find that the $PPFP_{11}\text{-}S$ scheme achieves a more accurate solution with less CPU time, which validates the simplified scheme, at least for this example. In addition, comparing the computation time of the $PPFP_{11}$ scheme with that of the P_{11} scheme, we can conclude

that the additional filtering term and positive-preserving limiters do not add too much computation time.

| Schemes | S_{16} | P_{11} | $PPFP_{11}^{1\text{-order}}$ | $PPFP_{11}$ | $PPFP_{11}\text{-}S$ |
|-------------------|----------|----------|------------------------------|-------------|----------------------|
| $re(\ell_2^\rho)$ | 5.31E-1 | 8.45E-1 | 9.29E-2 | 6.78E-2 | 5.79E-2 |
| CPU time (sec) | 210 | 868 | 247 | 882 | 220 |

Table 2: EXAMPLE 1. Relative error $re(\ell_2^\rho)$ and computation time by the various methods.

EXAMPLE 2 (**AP test**). This example is used to test the asymptotic preserving property of the proposed schemes in 1D. The problem specifications of this example are given in Table 3. In this simulation, we take 200 spatial meshes and time step $\Delta t = 0.1 \cdot \Delta x$. Since the solution for the given coefficient ϵ is generally not oscillatory, $PPFP_3$ and $PPFP_3\text{-}S$ with $\sigma_f = 0$ are used to discretize the angular variable.

Table 3: Problem specifications of EXAMPLE 2.

| | |
|----------------------|--|
| Spatial domain: | $[0, 1]$ |
| Parameters: | $\sigma = 1, c = 1, \epsilon = 10^{-8}$ |
| Boundary conditions: | $I(0, \mu, t) = 1$ for $\mu > 0$ $I(1, \mu, t) = 0$ for $\mu < 0$ |
| Initial condition: | $I(x, \mu, 0) = 0$ |

Figure 3 shows the computed results of $\bar{\rho}$ with $\bar{\rho} = \rho/(4\pi)$ at $t = 0.01, 0.05, 0.15, 2.0$. From Figure 3, we see that both $PPFP_3$ and $PPFP_3\text{-}S$ solutions agree well with the reference solution. This implies that in the optically thick regime, both $PPFP_N$ and $PPFP_N\text{-}S$ schemes can recover the diffusion solution accurately. Hence, this shows the *AP* property of the current schemes.

The following Example 3 is given in the non-dimensional form, and is designed to test the accuracy of the proposed schemes to the nonlinear gray radiative transfer problem.

EXAMPLE 3 (**Accuracy test**). This example aims at testing the spatial second-order accuracy of the proposed schemes in the regime $\epsilon \ll 1$ and the regime $\epsilon = O(1)$. Table 4 shows the problem specifications of this example. And the final simulation time of this example is taken to be $t = 0.2$.

$PPFP_7$ and $PPFP_7\text{-}S$ with $\sigma_f = 0$ are applied to discretize the angular variable for all given values of ϵ in this simulation. Remind that by setting $N = 7$ one is already able to resolve the angular variable accurately enough, thus $\sigma_f = 0$ is taken. And also in this setting, the errors of the schemes mainly come from the spatial and temporal discretization. Uniform spatial meshes are used with N_x denoting the number of spatial cells. In order to test the spatial accuracy, we take the time step to be $\Delta t = (\Delta x)^2$, which also satisfies the positive preserving constraint conditions and the CFL condition. Here

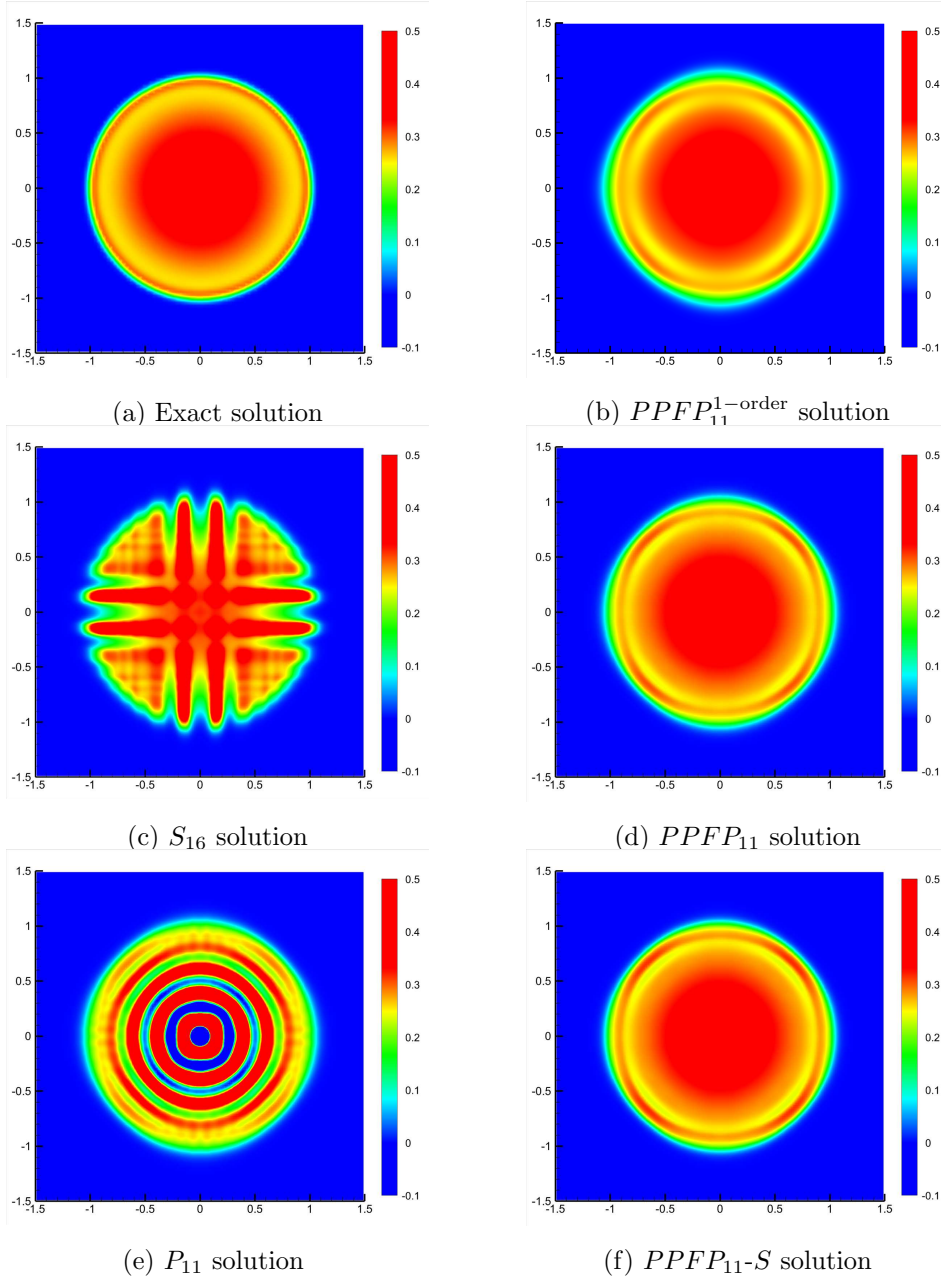
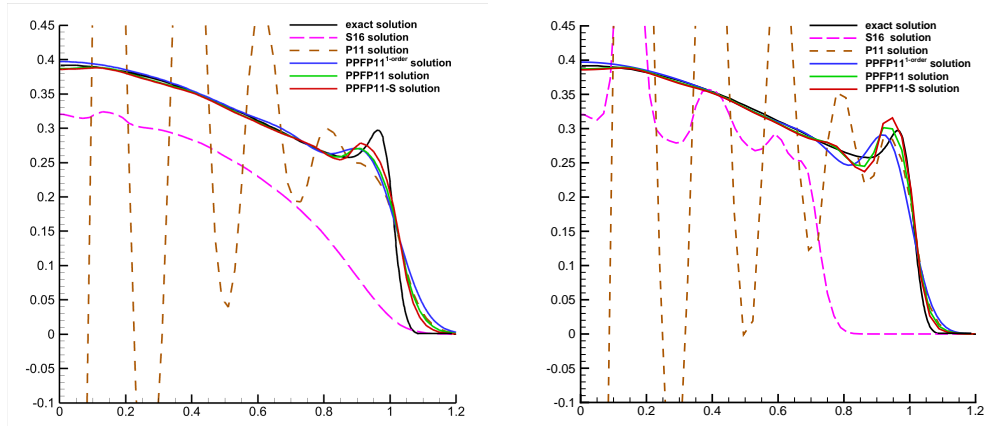


Figure 1: EXAMPLE 1. The solution ρ of the line source problem by the various methods.



(a) along x axis

(b) along $y = x$

Figure 2: EXAMPLE 1. The line-outs of ρ by various methods.

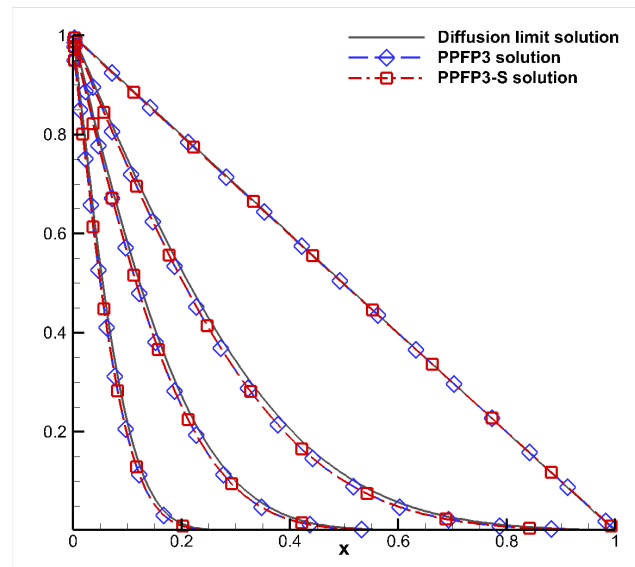


Figure 3: EXAMPLE 2. Linear kinetic transfer solution $\bar{\rho}$ at times 0.01, 0.05, 0.15, 2.0 (from left to right).

Table 4: Problem specifications of EXAMPLE 3.

| | |
|----------------------|---|
| Spatial domain: | $[0, 1]$ |
| Parameters: | $\sigma = 1, a = 1, c = 1, C_\nu = 1$ $\epsilon = 1, 10^{-1}, 10^{-6}, 10^{-9}$ respectively |
| Boundary conditions: | periodic boundary |
| Initial condition: | $T(x, 0) = 1 + \frac{1}{2}\sin(2\pi x)$ $I(x, \Omega, 0) = acT(x, 0)^4$ |

the numerical solution on a finer mesh $\Delta x/2$ is used as a reference solution to compute the relative L_2 and L_∞ errors of ρ and T on current mesh Δx . Tables 5-6 show the computed results. From these Tables we clearly observe the second-order accuracy for given values of ϵ . Thus, we have verify the spatial accuracy of the proposed schemes in the regimes $\epsilon \ll 1$ and $\epsilon = O(1)$.

In addition to the accuracy test, to test the asymptotic preserving property in this case, we denote the asymptotic preserving error by

$$err_{ap} = \max_{i,j} \left\{ \left| I_{0,i,j}^0 - \frac{\phi_{i,j}}{2\sqrt{\pi}} \right| + \sum_{1 \leq \ell \leq N, -\ell \leq m \leq \ell} |I_{\ell,i,j}^m| \right\}.$$

To see the behavior of the proposed schemes as $\epsilon \rightarrow 0$, we present the time evolution of the error err_{ap} in Figure 4. Note that the results are computed by using the $PPFP_7$ and $PPFP_7-S$ schemes with $\sigma_f = 0$, $N_x = 100$ and $\Delta t = 0.25\Delta x$. From Figure 4 we know that for any given small ϵ , the error decreases with time first, and then reaches a fixed steady state, the value of which is within machine error of the double precision operation used in the code. Moreover, for any one of the two schemes, as ϵ decreases, the error gets smaller at the beginning. It should be pointed out that the observed difference between $PPFP_7$ and $PPFP_7-S$ at early time is within the numerical error of the schemes. Thus, we demonstrate the asymptotic preserving property of the proposed $PPFP_N$ and $PPFP_N-S$ schemes.

The remaining examples are all for the nonlinear gray radiative transfer equations in the dimensional form, which are taken from Refs. [13, 29]. In the following, the light speed $c = 29.98$ cm/ns, the radiation constant $a = 0.01372$ GJ/(cm³*keV⁴) and $\epsilon = 1$.

EXAMPLE 4 (Marshak wave-2B). In this example, we take the temperature-dependent absorption/emission coefficient to be $\sigma = \frac{100}{T^3}$ cm²/g, the specific heat to be 0.1 GJ/g/keV, and the density to be 3.0 g/cm³. The initial material temperature T is set to be 10⁻⁶ keV. The computational domain is a two-dimensional slab [0cm, 1cm] × [0cm, 0.01cm]. A constant isotropic incident radiation intensity with a Planckian distribution at 1keV is kept on the left boundary. In the simulation, we take the spatial meshes to be 200 × 1. Since the solution for the given coefficient σ is generally not oscillatory, $PPFP_3$ and $PPFP_3-S$ with $\sigma_f = 0$ are used to discretize the angular variable. As for the time step, we take

| | | <i>PPFP₇</i> | | | | <i>PPFP₇-S</i> | | | |
|------------|-------|-------------------------|-------|----------------------------|-------|---------------------------|-------|----------------------------|-------|
| ϵ | N_x | $\text{re}(L_2^\rho)$ | order | $\text{re}(L_\infty^\rho)$ | order | $\text{re}(L_2^\rho)$ | order | $\text{re}(L_\infty^\rho)$ | order |
| 1 | 20 | 1.01E-02 | - | 1.31E-02 | - | 9.51E-03 | - | 1.30E-02 | - |
| | 40 | 3.59E-03 | 1.49 | 4.75E-03 | 1.46 | 3.43E-03 | 1.47 | 4.74E-03 | 1.46 |
| | 80 | 9.73E-04 | 1.88 | 1.42E-03 | 1.74 | 9.34E-04 | 1.88 | 1.41E-03 | 1.75 |
| | 160 | 2.59E-04 | 1.91 | 4.28E-04 | 1.73 | 2.49E-04 | 1.91 | 4.26E-04 | 1.73 |
| | 320 | 6.68E-05 | 1.95 | 1.13E-04 | 1.93 | 6.45E-05 | 1.95 | 1.12E-04 | 1.93 |
| 10^{-1} | 20 | 4.89E-03 | - | 8.44E-03 | - | 3.44E-02 | - | 4.27E-02 | - |
| | 40 | 2.97E-03 | 0.72 | 4.36E-03 | 2.02 | 7.87E-03 | 2.13 | 9.80E-03 | 2.12 |
| | 80 | 8.53E-04 | 1.80 | 1.28E-03 | 1.99 | 1.98E-03 | 1.99 | 2.46E-03 | 1.99 |
| | 160 | 2.27E-04 | 1.91 | 3.49E-04 | 1.99 | 4.95E-04 | 2.00 | 6.15E-04 | 2.00 |
| | 320 | 5.84E-05 | 1.96 | 9.08E-05 | 2.00 | 1.24E-04 | 2.00 | 1.53E-04 | 2.00 |
| 10^{-6} | 20 | 3.78E-03 | - | 6.42E-03 | - | 3.78E-03 | - | 6.42E-03 | - |
| | 40 | 3.45E-04 | 3.46 | 5.74E-04 | 3.48 | 3.45E-04 | 3.46 | 5.74E-04 | 3.48 |
| | 80 | 8.62E-05 | 2.00 | 1.43E-04 | 2.00 | 8.62E-05 | 2.00 | 1.43E-04 | 2.00 |
| | 160 | 2.16E-05 | 2.00 | 3.58E-05 | 2.00 | 2.16E-05 | 2.00 | 3.59E-05 | 2.00 |
| | 320 | 5.36E-06 | 2.01 | 8.89E-06 | 2.01 | 5.46E-06 | 1.98 | 9.11E-06 | 1.98 |
| 10^{-9} | 20 | 3.78E-03 | - | 6.42E-03 | - | 3.78E-03 | - | 6.42E-03 | - |
| | 40 | 3.45E-04 | 3.46 | 5.74E-04 | 3.48 | 3.45E-04 | 3.46 | 5.74E-04 | 3.48 |
| | 80 | 8.62E-05 | 2.00 | 1.43E-04 | 2.00 | 8.62E-05 | 2.00 | 1.43E-04 | 2.00 |
| | 160 | 2.16E-05 | 2.00 | 3.58E-05 | 2.00 | 2.16E-05 | 2.00 | 3.58E-05 | 2.00 |
| | 320 | 5.39E-06 | 2.00 | 8.96E-05 | 2.00 | 5.39E-06 | 2.00 | 8.96E-06 | 2.00 |

Table 5: EXAMPLE 3. Relative errors of ρ at $t = 0.2$.

$\Delta t = 0.7 \cdot \Delta x/c$ for the *PPFP₃* scheme and $\Delta t = 0.05 \cdot \Delta x/c$ for the *PPFP₃-S* scheme.

In Figure 5, we compare the radiation temperature $T_r \equiv (\frac{\rho}{ac})^{1/4}$ at times 15, 30, 45, 60, 74 ns computed by the current *PPFP₃* and *PPFP₃-S* schemes with those in [29] by S_6 . The numerical material temperatures T at time 74 ns are presented in Figure 6. In addition, the diffusion solution is also given in Figure 6 for comparison. From Figures 5-6, we clearly see that T_r and T computed by the current schemes show almost no difference with the S_6 solution in [29]. Moreover, the material temperatures agree well with the diffusion limit solution at 74 ns. This verifies that the proposed scheme can capture the right diffusive limit.

EXAMPLE 5 (Marshak wave-2A). The Marshak wave-2A problem is almost the same as the Marshak wave-2B problem except that the coefficient $\sigma = \frac{10}{7^3} \text{ cm}^2/\text{g}$. And also the same spatial meshes and angular discretization are used in the simulation of this problem. Here $\Delta t = 0.25 \cdot \Delta x/c$ is taken. Figures 7 and 8 show the numerical results of T_r and T . It can be seen from Figures 7-8 that the *PPFP₃* solution and *PPFP₃-S* solution agree well with the S_6 solution in [29]. But the computed material temperatures T of the current schemes are quite different from the diffusion limit solution, which is indeed the case since the small absorption/emission coefficient in this example violates the equilibrium diffusion approximation.

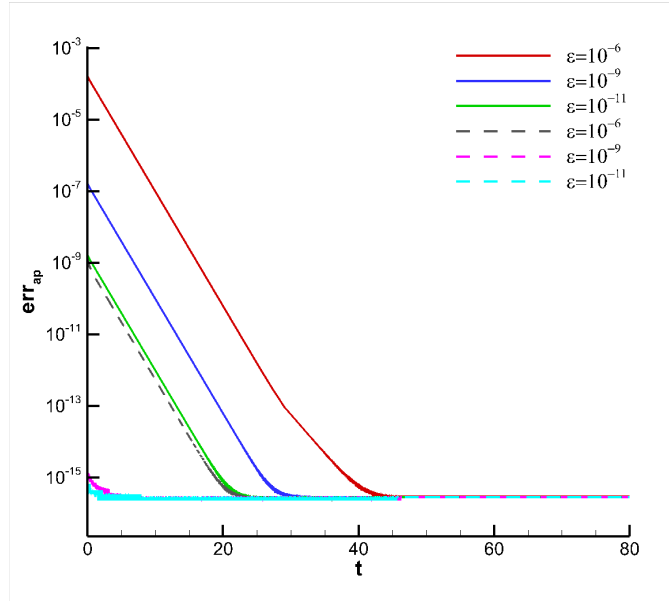


Figure 4: EXAMPLE 3. Time evolution of err_{ap} by the $PPFP_7$ scheme (solid line) and $PPFP_7-S$ scheme (dashed line).

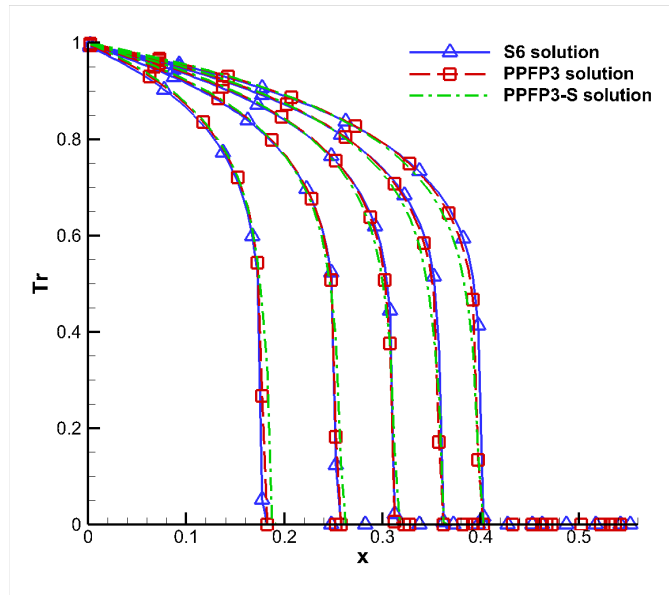


Figure 5: EXAMPLE 4. The radiation temperature T_r at times 15, 30, 45, 60, 74 ns (from left to right) for the Marshak wave-2B problem.

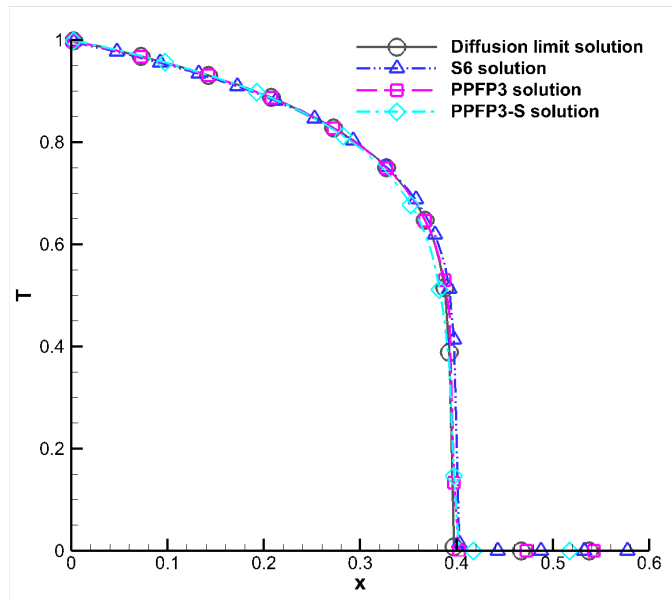


Figure 6: EXAMPLE 4. The numerical material temperature T at time 74 ns for the Marshak wave-2B problem.

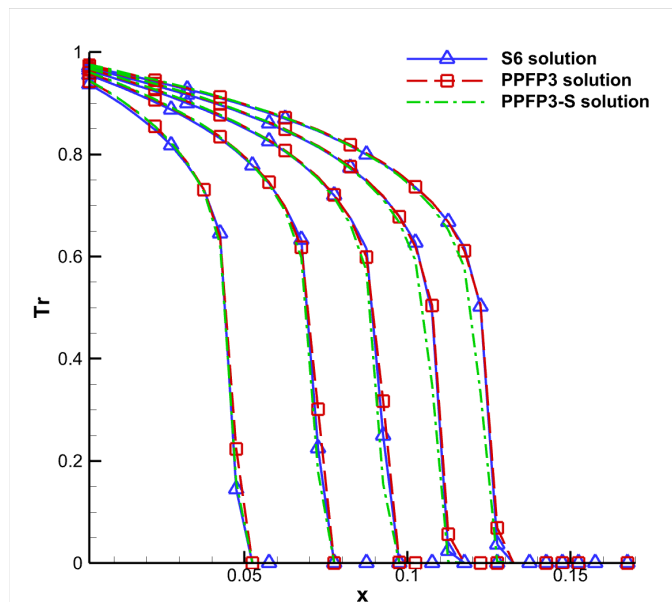


Figure 7: EXAMPLE 5. The radiation temperature T_r at times 0.2, 0.4, 0.6, 0.8, 1.0 ns (from left to right) for the Marshak wave-2A problem.

| | | $PPFP_7$ | | | | $PPFP_7-S$ | | | |
|------------|-------|-------------|-------|------------------|-------|-------------|-------|------------------|-------|
| ϵ | N_x | $re(L_2^T)$ | order | $re(L_\infty^T)$ | order | $re(L_2^T)$ | order | $re(L_\infty^T)$ | order |
| 1 | 20 | 3.32E-03 | - | 4.34E-03 | - | 3.18E-03 | - | 4.20E-03 | - |
| | 40 | 9.69E-04 | 1.78 | 1.23E-03 | 1.82 | 9.27E-04 | 1.78 | 1.20E-03 | 1.81 |
| | 80 | 2.50E-04 | 1.96 | 3.81E-04 | 1.69 | 2.39E-04 | 1.96 | 3.73E-04 | 1.69 |
| | 160 | 6.39E-05 | 1.97 | 1.07E-04 | 1.83 | 6.12E-05 | 1.96 | 1.05E-04 | 1.83 |
| | 320 | 1.62E-05 | 1.98 | 2.87E-05 | 1.90 | 1.55E-05 | 1.98 | 2.80E-05 | 1.90 |
| 10^{-1} | 20 | 1.35E-03 | - | 2.77E-03 | - | 8.97E-03 | - | 1.37E-02 | - |
| | 40 | 7.97E-04 | 0.76 | 1.45E-03 | 0.93 | 2.04E-03 | 2.14 | 3.08E-03 | 2.16 |
| | 80 | 2.28E-04 | 1.80 | 4.27E-04 | 1.77 | 5.13E-04 | 1.99 | 7.72E-04 | 2.00 |
| | 160 | 6.08E-05 | 1.91 | 1.17E-04 | 1.87 | 1.28E-04 | 2.00 | 1.92E-04 | 2.00 |
| | 320 | 1.56E-05 | 1.96 | 3.05E-05 | 1.94 | 3.21E-05 | 2.00 | 4.81E-05 | 2.00 |
| 10^{-6} | 20 | 9.83E-04 | - | 2.00E-03 | - | 9.83E-04 | - | 2.00E-03 | - |
| | 40 | 9.81E-05 | 3.33 | 2.46E-04 | 3.02 | 9.81E-05 | 3.33 | 2.46E-04 | 3.02 |
| | 80 | 2.45E-05 | 2.00 | 6.16E-05 | 2.00 | 2.45E-05 | 2.00 | 6.16E-05 | 2.00 |
| | 160 | 6.13E-06 | 2.00 | 1.54E-05 | 2.00 | 6.14E-06 | 2.00 | 1.54E-05 | 2.00 |
| | 320 | 1.52E-06 | 2.01 | 3.82E-06 | 2.01 | 1.56E-06 | 1.98 | 3.92E-06 | 1.98 |
| 10^{-9} | 20 | 9.83E-04 | - | 2.00E-03 | - | 9.83E-04 | - | 2.00E-03 | - |
| | 40 | 9.81E-05 | 3.33 | 2.46E-04 | 3.02 | 9.81E-05 | 3.46 | 2.46E-04 | 3.02 |
| | 80 | 2.45E-05 | 2.00 | 6.16E-05 | 2.00 | 2.45E-05 | 2.00 | 6.16E-05 | 2.00 |
| | 160 | 6.13E-06 | 2.00 | 1.54E-05 | 2.00 | 6.13E-06 | 2.00 | 1.54E-05 | 2.00 |
| | 320 | 1.53E-06 | 2.00 | 3.85E-06 | 2.00 | 1.53E-06 | 2.00 | 3.85E-06 | 2.00 |

Table 6: EXAMPLE 3. Relative errors of T at $t = 0.2$.

EXAMPLE 6 (**Tophat test**). The initial configuration of this problem is given in Figure 9. Initially, the radiation temperature and material temperature are taken to be 0.05keV everywhere. A heating source with a fixed temperature 0.5 keV is located on the left boundary for $-0.5 < y < 0.5$. We place five probes (A,B,C,D,E) in the thin opacity material, with the positions marked in Figure 9, to monitor the change of the temperature.

In the simulation, we take 128×64 spatial meshes and let $\Delta t = 0.25 \cdot \min\{\Delta x, \Delta y\}/c$. The $PPFP_7$ and $PPFP_7-S$ schemes, with Lanczos' filter function $f_{\text{Lanczos}}(\lambda) = \frac{\sin(\lambda)}{\lambda}$ and the space-dependent filter parameter σ_f that is given in the table of Figure 9, are applied. In Figure 10, we plot the time evolution of T and T_r at five probe points. The S_{16} and P_7 solutions are presented in Figure 10 for reference and comparison.

It can be seen from Figure 10 that the material temperatures T computed by $PPFP_7$, $PPFP_7-S$ and P_7 agree well with the reference solution of S_{16} at all probes. As for the radiative temperatures T_r , they coincide at probes A,B,D and E. But for the probe C, the P_7 solution is oscillating heavily between 0.1ns and 1ns, while the $PPFP_7$ and $PPFP_7-S$ schemes still give very accurate solutions.

In order to verify the positive preserving property of the proposed schemes, we present the contours of ρ and its minimal negative values in Figure 11 and Table 7, respectively. From Figure 11 and Table 7, we can conclude that the FP_7 scheme indeed can damp oscillations in the P_7 approximation, and make the negative solution less likely. In addition,

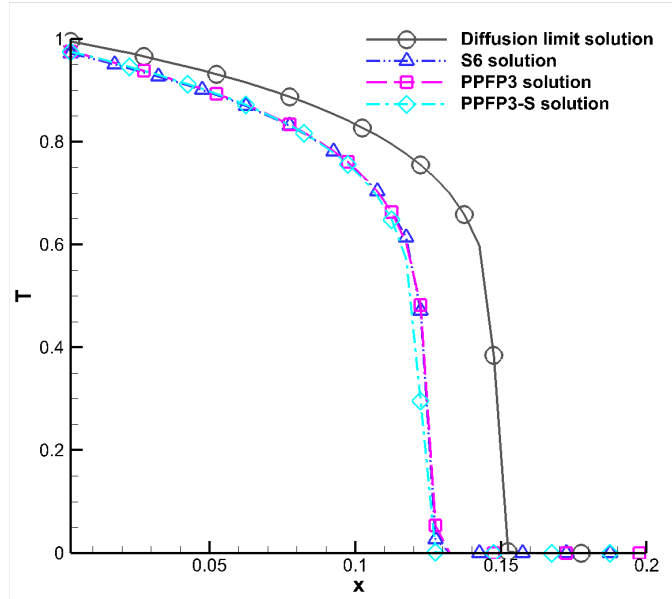


Figure 8: EXAMPLE 5. The material temperature T at time 1.0 ns for the Marshak wave-2A problem.

Figure 11 and Table 7 also show that, with the time evolution, the absolute value of the negative quantity decreases. However, a negative solution still appears in the FP_7 scheme. On the other hand, the solutions of the current $PPFP_7$ and $PPFP_7-S$ schemes are always positive. Moreover, the accuracy of both $PPFP_7$ and $PPFP_7-S$ solutions can be assured, which can be seen in comparison with the reference solution of P_{29} .

Figure 12 shows the contours of the computed material temperature T by the $PPFP_7$ and $PPFP_7-S$ schemes, from which we can see that there is almost no difference between them. Moreover, comparing them with the numerical results from [29], one can conclude that the current $PPFP_7$ and $PPFP_7-S$ schemes can still capture the interface between opacity thick and thin materials well.

| $\min \rho$ | P_7 | FP_7 | $PPFP_7$ | $PPFP_7-S$ |
|-----------------|----------|----------|----------|------------|
| at $t = 0.5$ ns | -2.32E-4 | -3.32E-5 | - | - |
| at $t = 1.0$ ns | -1.85E-4 | -3.73E-6 | - | - |

Table 7: EXAMPLE 6. Minimal negative values of the radiative energy density ρ .

7 Conclusion

In this paper, we have extended the previous first-order positive and asymptotic preserving FP_N scheme for the nonlinear gray radiative transfer equations [39] to a spatial second-order accuracy one. The scheme applies the filtered spherical harmonics approach to discretize the angular variable, and UGKS to discretize the time and spatial variables.

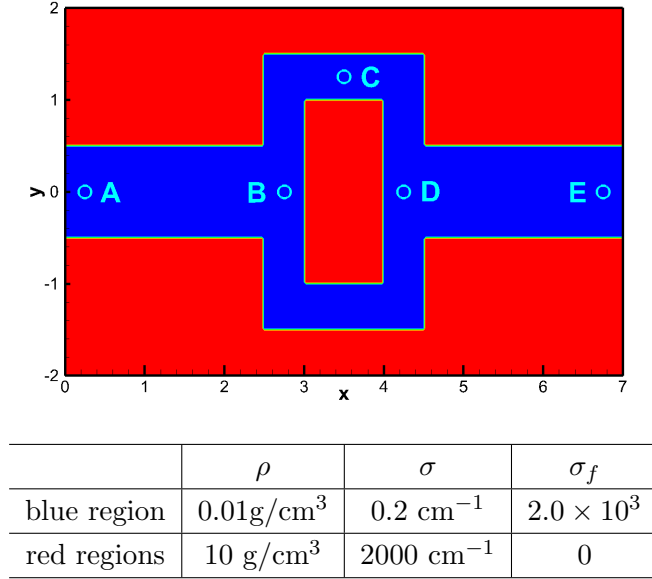


Figure 9: EXAMPLE 6. Initial configuration of the Tophat test problem.

Due to the FP_N angular discretization, the scheme is almost free of ray effects. It, meanwhile, can reduce the Gibbs phenomena by the filter term. In the spirit of UGKS, it is easy to show that the scheme is AP. Moreover, through a detailed analysis of the spatial second order fluxes which are obtained by using the IMC linearization method, we are able to find the sufficient conditions that guarantee the positivity of the radiative energy density and material temperature. Finally, by employing much cheap linear scaling limiters to make these conditions hold, the desired spatial second-order positive and asymptotic preserving scheme, i.e., the $PPFP_N$ -based UGKS, is obtained. The numerical examples validate the spatial second-order accuracy of the scheme as expected. Furthermore, in

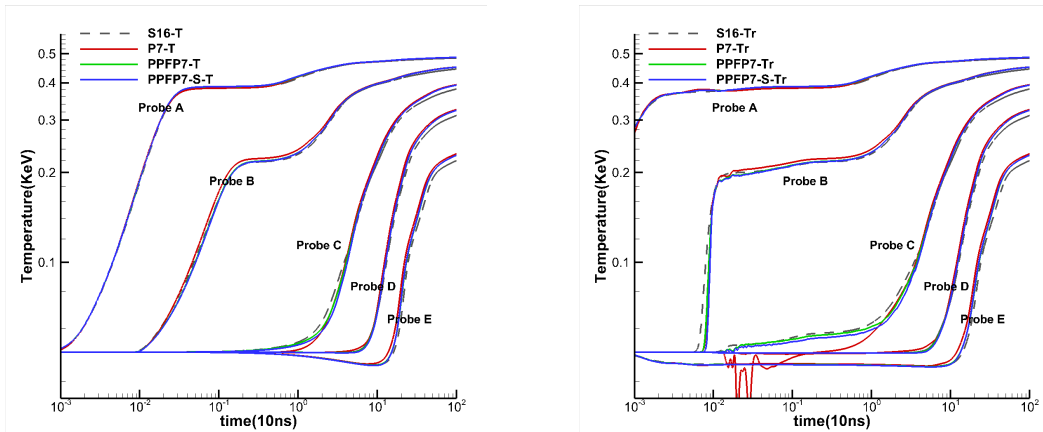


Figure 10: EXAMPLE 6. The time evolution of T and T_r at five probe points. The temperature unit is keV and the time unit is 10 ns.

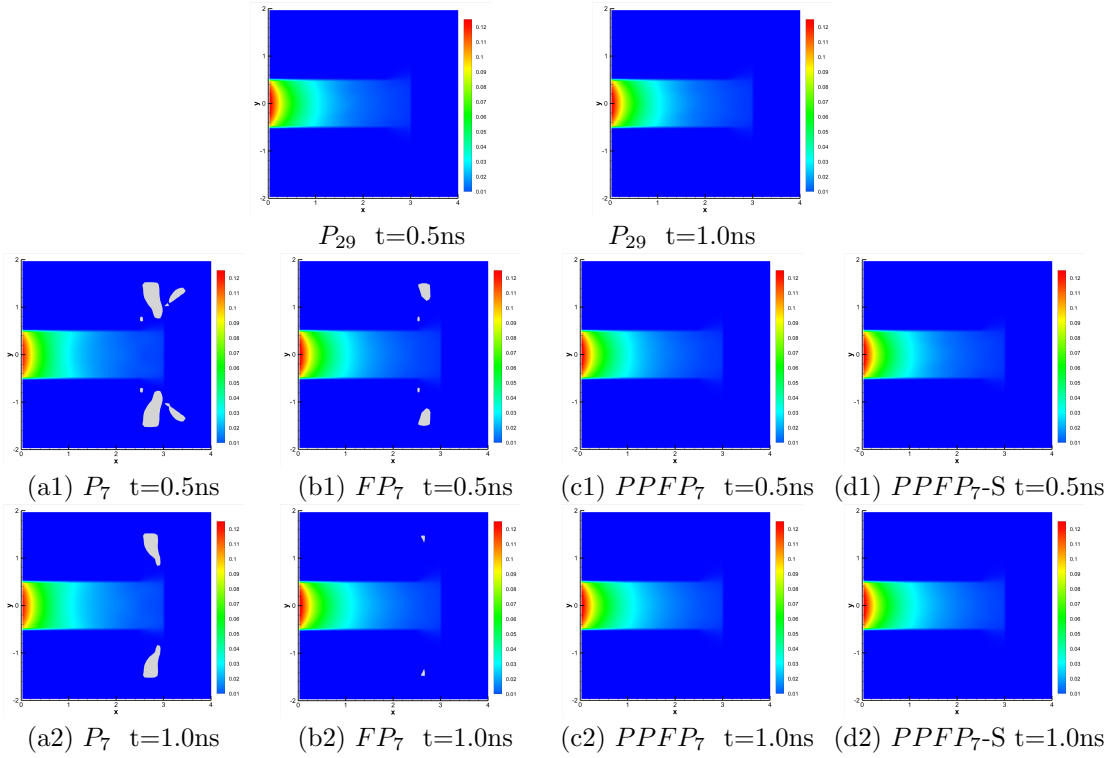


Figure 11: EXAMPLE 6. Contour of ρ . In the white regions ρ becomes negative.

order to reduce the computational costs of the fluxes in $PPFP_N$ -based UGKS in the regimes $\epsilon \ll 1$ and $\epsilon = O(1)$, a simplified version, called the $PPFP_N$ -based SUGKS, is presented.

To our best knowledge, this is the first time that a spatial second-order positive, asymptotic preserving and almost free of ray effects scheme has been constructed for the nonlinear radiative transfer equations without operator splitting. A number of standard (benchmark) problems have been tested to validate all the mentioned properties of the proposed schemes.

Acknowledgements

The current research is supported by NSFC (Grant No. 12001451) for Xu, and by National Key R&D Program (2020YFA0712200), and National Key Project (GJXM92579), the Sino-German Science Center (Grant No. GZ 1465) and the ISF-NSFC joint research program (Grant No. 11761141008) for Jiang, and by National Key Project (GJXM92579) for Sun.

8 Appendix. Proof of Lemma 5.1

In this appendix, we show the inequalities (5.1)-(5.4) in Lemma 5.1.

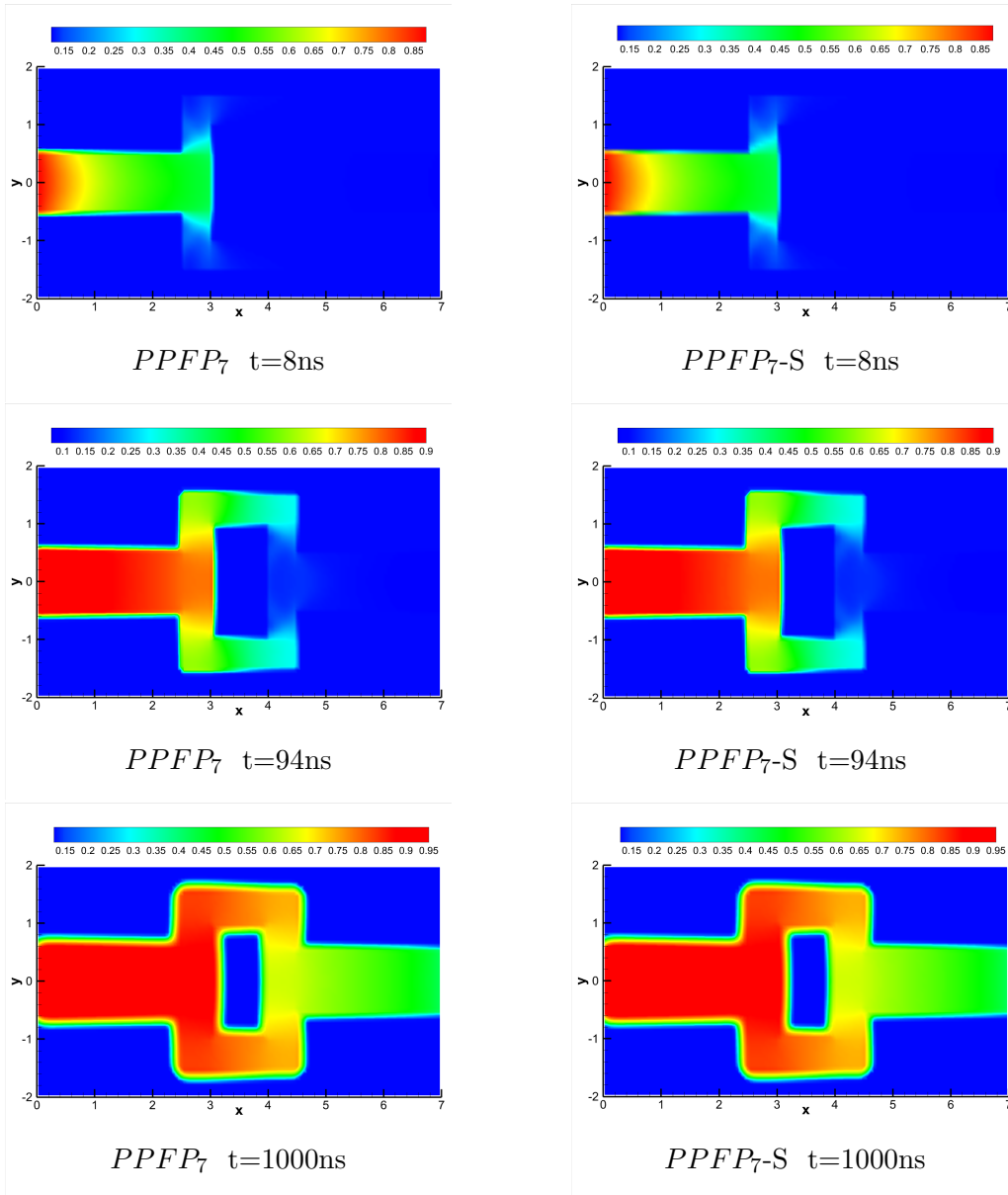


Figure 12: EXAMPLE 6. Contours of T . The temperature unit is 0.5 keV.

Proof of (5.1):

After a straightforward calculation, we have

$$\begin{aligned}
& \left| \frac{\Phi_{i-1/2,j}^{n+1}(\tilde{b}) - \Phi_{i+1/2,j}^{n+1}(\tilde{b})}{\Delta x} \right| \\
&= \left| \frac{\tilde{b}_{i-1/2,j}^{n+1} \left(\langle \xi^2 \vec{\psi} \rangle_{1,4} \cdot \delta_x \vec{I}_{i-1,j}^n + \langle \xi^2 \vec{\psi} \rangle_{2,3} \cdot \delta_x \vec{I}_{i,j}^n \right)}{\Delta x} \right. \\
&\quad \left. - \frac{\tilde{b}_{i+1/2,j}^{n+1} \left(\langle \xi^2 \vec{\psi} \rangle_{1,4} \cdot \delta_x \vec{I}_{i,j}^n + \langle \xi^2 \vec{\psi} \rangle_{2,3} \cdot \delta_x \vec{I}_{i+1,j}^n \right)}{\Delta x} \right| \\
&= \left| \langle \xi^2 \vec{\psi} \rangle_{1,4} \cdot \frac{\tilde{b}_{i-1/2,j}^{n+1} \delta_x \vec{I}_{i-1,j}^n - \tilde{b}_{i+1/2,j}^{n+1} \delta_x \vec{I}_{i,j}^n}{\Delta x} + \langle \xi^2 \vec{\psi} \rangle_{2,3} \cdot \frac{\tilde{b}_{i-1/2,j}^{n+1} \delta_x \vec{I}_{i,j}^n - \tilde{b}_{i+1/2,j}^{n+1} \delta_x \vec{I}_{i+1,j}^n}{\Delta x} \right| \\
&= \left| \langle \xi^2 \vec{\psi} \rangle_{1,4} \cdot \frac{\tilde{b}_{i-1/2,j}^{n+1} \left(\delta_x \vec{I}_{i-1,j}^n - \delta_x \vec{I}_{i,j}^n \right) + \left(\tilde{b}_{i-1/2,j}^{n+1} - \tilde{b}_{i+1/2,j}^{n+1} \right) \delta_x \vec{I}_{i,j}^n}{\Delta x} \right. \\
&\quad \left. + \langle \xi^2 \vec{\psi} \rangle_{2,3} \cdot \frac{\tilde{b}_{i-1/2,j}^{n+1} \left(\delta_x \vec{I}_{i,j}^n - \delta_x \vec{I}_{i+1,j}^n \right) + \left(\tilde{b}_{i-1/2,j}^{n+1} - \tilde{b}_{i+1/2,j}^{n+1} \right) \delta_x \vec{I}_{i+1,j}^n}{\Delta x} \right|. \tag{8.1}
\end{aligned}$$

We assume that there are smooth vector functions $\vec{I}(x, y, t)$ (here we have slightly abused the notation), such that

$$\vec{I}_{i,j}^n = \vec{I}(x_i, y_j, t_n).$$

Substituting \vec{I} and the coefficient function \tilde{b} into (8.1), we use the differential mean value theorem to find that for any component I_ℓ^m of \vec{I} and \tilde{b} , there are $(\zeta_x^1)_\ell^m, (\zeta_x^2)_\ell^m, \zeta_x$, such that

$$\begin{aligned}
\frac{\delta_x (I_\ell^m)_{i-1,j}^n - \delta_x (I_\ell^m)_{i,j}^n}{\Delta x} &= -\frac{\partial^2 (I_\ell^m)^n((\zeta_x^1)_\ell^m, y_j)}{\partial x^2}, \\
\frac{\delta_x (I_\ell^m)_{i,j}^n - \delta_x (I_\ell^m)_{i+1,j}^n}{\Delta x} &= -\frac{\partial^2 (I_\ell^m)^n((\zeta_x^2)_\ell^m, y_j)}{\partial x^2}, \\
\frac{\tilde{b}_{i-1/2,j}^{n+1} - \tilde{b}_{i+1/2,j}^{n+1}}{\Delta x} &= -\frac{\partial \tilde{b}^{n+1}(\zeta_x, y_j)}{\partial x}.
\end{aligned}$$

For convenience, denote

$$\frac{\partial^2 \vec{I}^n(\zeta_x^1, y_j)}{\partial x^2} = \left(\frac{\partial^2 (I_0^0)^n((\zeta_x^1)_0^0, y_j)}{\partial x^2}, \frac{\partial^2 (I_1^{-1})^n((\zeta_x^1)_1^{-1}, y_j)}{\partial x^2}, \dots, \frac{\partial^2 (I_N^N)^n((\zeta_x^1)_N^N, y_j)}{\partial x^2} \right)',$$

and analogously for $\frac{\partial^2 \vec{I}^n(\zeta_x^2, y_j)}{\partial x^2}$.

Therefore, one has

$$\begin{aligned}
& \left| \frac{\Phi_{i-1/2,j}^{n+1}(\tilde{b}) - \Phi_{i+1/2,j}^{n+1}(\tilde{b})}{\Delta x} \right| \\
&= \left| \langle \xi^2 \vec{\psi} \rangle_{1,4} \cdot \left(-\tilde{b}_{i-1/2,j}^{n+1} \frac{\partial^2 \vec{I}^n(\zeta_x^1, y_j)}{\partial x^2} - \frac{\partial \tilde{b}^{n+1}(\zeta_x, y_j)}{\partial x} \delta_x \vec{I}_{i,j}^n \right) \right. \\
&\quad \left. + \langle \xi^2 \vec{\psi} \rangle_{2,3} \cdot \left(-\tilde{b}_{i-1/2,j}^{n+1} \frac{\partial^2 \vec{I}^n(\zeta_x^2, y_j)}{\partial x^2} - \frac{\partial \tilde{b}^{n+1}(\zeta_x, y_j)}{\partial x} \delta_x \vec{I}_{i+1,j}^n \right) \right| \\
&\lesssim \left| \tilde{b}_{i-1/2,j}^{n+1} \right| + \left| \frac{\partial \tilde{b}^{n+1}(\zeta_x, y_j)}{\partial x} \right|.
\end{aligned}$$

In the same manner, we can obtain

$$\left| \frac{\Phi_{i,j-1/2}^{n+1}(\tilde{b}) - \Phi_{i,j+1/2}^{n+1}(\tilde{b})}{\Delta y} \right| \lesssim \left| \tilde{b}_{i,j-1/2}^{n+1} \right| + \left| \frac{\partial \tilde{b}^{n+1}(x_i, \zeta_y)}{\partial y} \right|.$$

Now, it remains to analyze \tilde{b} , $\frac{\partial \tilde{b}}{\partial x}$, $\frac{\partial \tilde{b}}{\partial y}$. After a straightforward calculation, one obtains

$$\frac{\partial \tilde{b}}{\partial x} = \frac{2c^2}{\epsilon^2 \Delta t \nu^3} \frac{\partial \nu}{\partial x} (1 - e^{-\nu \Delta t} - \nu \Delta t e^{-\nu \Delta t}) - \frac{c^2 \Delta t}{\epsilon^2 \nu} \frac{\partial \nu}{\partial x} e^{-\nu \Delta t},$$

where we recall $\nu = \frac{c\sigma}{\epsilon^2}$. Similarly, we have an identity for $\frac{\partial \tilde{b}}{\partial y}$.

Considering the regime $\epsilon \ll 1$ in which $\sigma = O(1)$, we can verify that

$$\left| \tilde{b} \right| = O\left(\frac{\epsilon^2}{\Delta t}\right), \quad \left| \frac{\partial \tilde{b}}{\partial x} \right| \ll \epsilon^2, \quad \left| \frac{\partial \tilde{b}}{\partial y} \right| \ll \epsilon^2.$$

On the other hand, for the regime $\epsilon = O(1)$, by the Taylor expansion, we have

$$\tilde{b} = O(\Delta t), \quad \frac{\partial \tilde{b}}{\partial x} = 0 \text{ or } O((\Delta t)^2), \quad \frac{\partial \tilde{b}}{\partial y} = 0 \text{ or } O((\Delta t)^2).$$

Putting the above analyses together and noticing that $\epsilon \ll \Delta t$, we obtain (5.1) immediately. This completes the proof of inequality (5.1).

Proof of (5.2):

In view of the expressions of $\Phi_{i-1/2,j}(\tilde{b})$ and $G_{i-1/2,j}(\tilde{b})$, one finds that the proof of the inequality (5.2) is almost the same as that of (5.1), and hence, we omit it here.

Proof of (5.3) and (5.4):

A straightforward calculation leads to

$$\begin{aligned}
& \left| \frac{G_{i-1/2,j}(\tilde{c}) - G_{i+1/2,j}(\tilde{c})}{\Delta x} \right| \\
&= \left| \frac{\tilde{c}_{i-1/2,j}^{n+1} \langle \xi \psi_\ell^m \rangle \left((\kappa^{n+1} \phi^n)_{i-1/2,j} + (1 - \kappa_{i-1/2,j}^{n+1}) \rho_{i-1/2,j}^{n+1} \right)}{\Delta x} \right. \\
&\quad \left. - \frac{\tilde{c}_{i+1/2,j}^{n+1} \langle \xi \psi_\ell^m \rangle \left((\kappa^{n+1} \phi^n)_{i+1/2,j} + (1 - \kappa_{i+1/2,j}^{n+1}) \rho_{i+1/2,j}^{n+1} \right)}{\Delta x} \right| \\
&= \left| \langle \xi \psi_\ell^m \rangle \left\{ \frac{\tilde{c}_{i-1/2,j}^{n+1} (\kappa^{n+1} \phi^n)_{i-1/2,j} - \tilde{c}_{i+1/2,j}^{n+1} (\kappa^{n+1} \phi^n)_{i+1/2,j}}{\Delta x} \right. \right. \\
&\quad \left. \left. + \frac{\tilde{c}_{i-1/2,j}^{n+1} (1 - \kappa_{i-1/2,j}^{n+1}) \rho_{i-1/2,j}^{n+1} - \tilde{c}_{i+1/2,j}^{n+1} (1 - \kappa_{i+1/2,j}^{n+1}) \rho_{i+1/2,j}^{n+1}}{\Delta x} \right\} \right|. \tag{8.2}
\end{aligned}$$

We suppose that there are smooth functions $\phi(x, y, t), \rho(x, y, t)$, such that

$$\phi_{i,j}^n = \phi(x_i, y_j, t_n), \quad \rho_{i,j}^n = \rho(x_i, y_j, t_n).$$

Substituting ϕ, ρ and the coefficient function \tilde{c} into (8.2), using the differential mean value theorem, we see that there are ζ_x^1, ζ_x^2 , such that

$$\begin{aligned}
& \left| \frac{G_{i-1/2,j}(\tilde{c}) - G_{i+1/2,j}(\tilde{c})}{\Delta x} \right| \\
&= \left| \langle \xi \psi_\ell^m \rangle \frac{\partial(\tilde{c}^{n+1} \kappa^{n+1} \phi^n)}{\partial x}(\zeta_x^1, y_j) + \frac{\partial(\tilde{c}^{n+1} (1 - \kappa^{n+1}) \rho^{n+1})}{\partial x}(\zeta_x^2, y_j) \right| \\
&\lesssim \max_{k=1,2} \left| \tilde{c}^{n+1}(\zeta_x^k, y_j) \right| + \max_{k=1,2} \left| \frac{\partial \tilde{c}^{n+1}}{\partial x}(\zeta_x^k, y_j) \right|.
\end{aligned}$$

Similarly,

$$\left| \frac{G_{i,j-1/2}(\tilde{c}) - G_{i,j+1/2}(\tilde{c})}{\Delta y} \right| \lesssim \max_{k=1,2} \left| \tilde{c}^{n+1}(x_i, \zeta_y^k) \right| + \max_{k=1,2} \left| \frac{\partial \tilde{c}^{n+1}}{\partial y}(x_i, \zeta_y^k) \right|.$$

Now, we focus on estimating $\tilde{c}, \frac{\partial \tilde{c}}{\partial x}$ and $\frac{\partial \tilde{c}}{\partial y}$. After a straightforward calculation, one has

$$\begin{aligned}
\frac{\partial \tilde{c}}{\partial x} &= \left(\frac{1}{2\pi\epsilon^3\nu} - \frac{1}{2\pi\Delta t\epsilon^3\nu^2} (1 - e^{-\nu\Delta t}) \right) \frac{\partial \sigma_s}{\partial x} \\
&\quad + \left(\frac{\sigma_s}{\pi\Delta t\epsilon^3\nu^3} (1 - e^{-\nu\Delta t}) - \frac{\sigma_s}{2\pi\epsilon^3\nu^2} (1 + e^{-\nu\Delta t}) \right) \frac{\partial \nu}{\partial x}.
\end{aligned}$$

A similar identity for $\frac{\partial \tilde{c}}{\partial y}$ can be obtained in the same manner.

Consider the regime $\epsilon \ll 1$ where $\sigma = O(1)$. When $\sigma = \text{const.}$, we see that $\frac{\partial \sigma}{\partial x} = 0$; otherwise, $\frac{\partial \sigma}{\partial x} = O(1)$. Thus, it is easy to verify that

$$\tilde{c} = O\left(\frac{1}{\epsilon}\right), \quad \frac{\partial \tilde{c}}{\partial x} = 0 \text{ or } O\left(\frac{1}{\epsilon}\right), \quad \frac{\partial \tilde{c}}{\partial y} = 0 \text{ or } O\left(\frac{1}{\epsilon}\right).$$

On the other hand, for the regime $\epsilon = O(1)$, we employ the Taylor expansion and argue similarly to arrive at

$$\tilde{c} = O(\Delta t), \quad \frac{\partial \tilde{c}}{\partial x} = 0 \text{ or } O(\Delta t), \quad \frac{\partial \tilde{c}}{\partial y} = 0 \text{ or } O(\Delta t).$$

Hence, recalling $\epsilon \ll \Delta t$, we get (5.3) and (5.4). This completes the proof of Lemma 5.1.

References

- [1] M. Benassi, R.D.M. Garcia, A.H. Karp, C.E. Siewert, A high-order spherical harmonics solution to the standard problem in radiative transfer. *The Astrophysical Journal*, 280(1984): 853-864.
- [2] L.L. Briggs, W.F. Miller Jr, E.E. Lewis, Ray-effect mitigation in discrete ordinate-like angular finite element approximations in neutron transport, *Nuclear Science and Engineering*, 57(1975): 205-217.
- [3] A.G. Buchan, C.C. Pain, M.D. Eaton, R.P. Smedley-Stevenson, A.J.H. Goddard, Linear and quadratic octahedral wavelets on the sphere for angular discretisations of the Boltzmann transport equation, *Annals of Nuclear Energy*, 32(2005): 1224-1273.
- [4] R.O. Castro, J.P. Trelles, Spatial and angular finite element method for radiative transfer in participating media, *Journal of Quantitative Spectroscopy and Radiative Transfer*, 157(2015): 81-105.
- [5] J.C. Chai, S.V. Patankar, H.S. Lee, Evaluation of spatial differencing practices for the discrete-ordinates method, *J. Thermophys. Heat Transfer*, 8(1994): 140-144.
- [6] J. Fleck, J. Cummings, An implicit monte carlo scheme for calculating time and frequency dependent nonlinear radiation transport. *Journal of Computational Physics* 8(1971), 313-342.
- [7] Y.W. Fan, R. Li, L.C. Zheng, A nonlinear moment model for radiative transfer equation in slab geometry, *Journal of Computational Physics*, 404 (2020): 109128.
- [8] F. Filbet, S. Jin, A class of asymptotic-preserving schemes for kinetic equations and related problems with stiff sources, *Journal of Computational Physics*, 229(2010): 7625-7648.
- [9] C.K. Garrett, C.D. Hauck, A comparison of moment closures for linear kinetic transport equations, the line source benchmark, *Transport Theory and Statistical Physics*, 42(2013): 203-235.
- [10] B.D. Ganapol, Homogeneous infinite media time-dependent analytic benchmarks for XTM transport methods development, Technical Report, Los Alamos National Laboratory, Los Alamos, NM, 1999.
- [11] M.A. Goffin, A.G. Buchan, S. Dargaville, C.C. Pain, et al, Goal-based angular adaptivity applied to a wavelet-based discretisation of the neutral particle transport equation, *Journal of Computational Physics*, 281(2015): 1032-1062.

- [12] J.L. Guermond, B. Popov, J. Ragusa, Positive and asymptotic preserving approximation of the radiation transport equation, *SIAM Journal on Numerical Analysis*, 58(2020): 519-540.
- [13] N.A. Gentile, Implicit Monte Carlo diffusion-an acceleration method for Monte Carlo time-dependent radiative transfer simulations, *Journal of Computational Physics*, 172(2001): 543-571.
- [14] C. Hauck, R. McClarren, Positive PN closures, *SIAM Journal on Scientific Computing*, 32(2010): 2603-2626.
- [15] J.W. Hu, R.W. Shu, A second-order asymptotic-preserving and positivity-preserving exponential runge-kutta method for a class of stiff kinetic equations, *Multiscale Model Simul*, 17(2019): 1123-1146.
- [16] S. Jin, Asymptotic preserving (AP) schemes for multiscale kinetic and hyperbolic equations: a review, *Lecture notes for summer school on methods and models of kinetic theory (M&MKT)*, Porto Ercole (Grosseto, Italy), 2010: 177-216.
- [17] E.W. Larsen, G.C. Pomraning, V.C. Badham, Asymptotic analysis of radiative transfer problems, *Journal of Quantitative Spectroscopy and Radiative Transfer*, 29(1983): 285-310.
- [18] E.W. Larsen, J.E. Morel, W.F. Miller Jr, Asymptotic solutions of numerical transport problems in optically thick, diffusive regimes, *Journal of Computational Physics*, 69(1987): 283-324.
- [19] A.W. Larsen, J.E. Morel, Asymptotic solutions of numerical transport problems in optically thick, diffusive regimes. II, *Journal of Computational Physics*, 83(1)(1989): 212-236.
- [20] M.P. Laiu, C.D. Hauck, Positivity limiters for filtered spectral approximations of linear kinetic transport equations, *Journal of Scientific Computing*, 78(2019): 918-950.
- [21] M.P. Laiu, M. Frank, C.D. Hauck, A positive asymptotic-preserving scheme for linear kinetic transport equations, *SIAM Journal on Scientific Computing*, 41(2019): A1500-A1526.
- [22] M.P. Laiu, C.D. Hauck, R.G. McClarren, D.P. OLeary, Positive filtered P_N moment closures for linear kinetic equations, *SIAM Journal on Numerical Analysis*, 54(2016): 3214-3238.
- [23] E.E. Lewis, W.F. Miller, *Computational methods of neutron transport*, New York, (1984): 401pp.
- [24] D. Ling, J. Cheng, C.W. Shu, Conservative high order positivity-preserving discontinuous galerkin methods for linear hyperbolic and radiative transfer equations, *Journal of Scientific Computing*, 77(2018): 1801-1831.
- [25] R.G. McClarren, J.P. Holloway, T.A. Brunner, On solutions to the Pn equations for thermal radiative transfer, *Journal of Computational Physics*, 227(2008): 2864-2885.
- [26] R.G. McClarren, C.D. Hauck, Robust and accurate filtered spherical harmonics expansions for radiative transfer, *Journal of Computational Physics*, 229(2010): 5597-5614.

- [27] L. Mieussens, On the asymptotic preserving property of the unified gas kinetic scheme for the diffusion limit of linear kinetic models, *Journal of Computational Physics*, 253(2013): 138-156.
- [28] D. Radice, E. Abdikamalov, L. Rezzolla, C.D. Ott, A new spherical harmonics scheme for multi-dimensional radiation transport I. Static matter configurations, *Journal of Computational Physics*, 242(2013): 648-669.
- [29] W.J. Sun, S. Jiang, K. Xu, An asymptotic preserving unified gas kinetic scheme for gray radiative transfer equations, *Journal of Computational Physics*, 285(2015): 265-279.
- [30] W.J. Sun, S. Jiang, K. Xu, An asymptotic preserving unified gas kinetic scheme for frequency-dependent radiative transfer equations, *Journal of Computational Physics*, 302(2015): 222-238.
- [31] W.J. Sun, S. Jiang, K. Xu, An asymptotic preserving implicit unified gas kinetic scheme for frequency-dependent radiative transfer equations, *International Journal of Numerical Analysis and Modeling*, 15(2018): 134-153.
- [32] W.J. Sun, S. Jiang, K. Xu, An implicit unified gas kinetic scheme for radiative transfer with equilibrium and non-equilibrium diffusive limits, *Communications in Computational Physics*, 22(2017): 889-912.
- [33] W.J. Sun, S. Jiang, K. Xu, A multidimensional unified gas-kinetic scheme for radiative transfer equations on unstructured mesh, *Journal of Computational Physics*, 351(2017): 455-472.
- [34] L. Soucasse, S. Dargaville, A.G. Buchan, C.C. Pain, A goal-based angular adaptivity method for thermal radiation modelling in non grey media, *Journal of Quantitative Spectroscopy and Radiative Transfer*, 200(2017): 215-224.
- [35] T.A. Wareing, An exponential discontinuous scheme for discrete-ordinate calculations in Cartesian geometries, in *Proceedings of the Joint International Conference on Mathematical Methods and Supercomputing for Nuclear Applications*, Saratoga Springs, NY 1997.
- [36] T. Xiong, W.J. Sun, Y. Shi, P. Song, High order asymptotic preserving discontinuous Galerkin methods for gray radiative transfer equations, *Journal of Computational Physics*, 463(2022): 111308.
- [37] K. Xu, J.C. Huang, A unified gas-kinetic scheme for continuum and rarefied flows, *Journal of Computational Physics*, 229(2010): 7747-7764.
- [38] X.J. Xu, W.J. Sun, S. Jiang, An asymptotic preserving angular finite element based unified gas kinetic scheme for gray radiative transfer equations, *Journal of Quantitative Spectroscopy and Radiative Transfer*, 243(2020): 106808, 13pp.
- [39] X.J. Xu, S. Jiang, W.J. Sun, A positive and asymptotic preserving filtered P_N method for the gray radiative transfer equations, *Journal of Computational Physics*, 444(2021) 110546.
- [40] X.J. Xu, S. Jiang, W.J. Sun, Spatial second-order positive and asymptotic preserving unified gas kinetic schemes for radiative transfer equations, submitted.

- [41] D.M. Yuan, J. Cheng, C.W. Shu, High order positivity-preserving discontinuous Galerkin methods for radiative transfer equations, *SIAM J. Sci. Comput.* 38(2016): A2987-A3019.
- [42] X.X. Zhang, C.W. Shu, On maximum-principle-satisfying high order schemes for scalar conservation laws, *Journal of Computational Physics*, 229(2010): 3091-3120.